Published by Institute of Physics Publishing for SISSA

Received: *April 10, 2007*
Accepted: *April 21, 2007*
Published: *May 16, 2007*

Black saturn

Henriette Elvang

Center for Theoretical Physics,
Massachusetts Institute of Technology, Cambridge, MA 02139, U.S.A.
E-mail: elvang@lns.mit.edu

Pau Figueras

Departament de Física Fonamental, Universitat de Barcelona,
Diagonal 647, E-08028, Barcelona, Spain
E-mail: pfigueras@ffn.ub.es

Abstract: Using the inverse scattering method we construct an exact stationary asymptotically flat 4+1-dimensional vacuum solution describing "black saturn": a spherical black hole surrounded by a black ring. Angular momentum keeps the configuration in equilibrium. Black saturn reveals a number of interesting gravitational phenomena: (1) The balanced solution exhibits 2-fold continuous non-uniqueness for fixed mass and angular momentum; (2) Remarkably, the 4+1d Schwarzschild black hole is not unique, since the black ring and black hole of black saturn can counter-rotate to give zero total angular momentum at infinity, while maintaining balance; (3) The system cleanly demonstrates rotational frame-dragging when a black hole with vanishing Komar angular momentum is rotating as the black ring drags the surrounding spacetime. Possible generalizations include multiple rings of saturn as well as doubly spinning black saturn configurations.

Keywords: Black Holes in String Theory, Black Holes, Integrable Equations in Physics.

JHEP05(2007)050

Contents

JHEP05(2007)050

1. Introduction

Multi-black hole spacetimes play an interesting role in black hole physics. A central question is how to keep a configuration of multiple black holes in equilibrium. Two Schwarzschild black holes attract each other and cannot be in equilibrium without external forces to hold them in place. The simplest way to achieve a stationary balanced configuration is by adding enough electric charge to each black hole, so that the electromagnetic repulsion exactly cancels the gravitational attraction. In 3+1 dimensions, the resulting solution, and its generalization to multiple black holes, is of course the well-known extremal multi-Reissner Nordstrom black hole solution [1].

For asymptotically flat vacuum solutions, rotation seems to be the only candidate for keeping black holes apart. However, for the 3+1-dimensional axisymmetric double Kerr solution [2], the spin-spin interaction [3] is not sufficiently strong to balance the gravitational attraction of black holes with regular horizons [4 – 7]. Hence multi-Kerr black hole spacetimes are not in equilibrium, but suffer from singular struts which provide the pressure to keep the black holes apart [5].

We present here a 4+1-dimensional stationary vacuum solution for which angular momentum does provide sufficient force to keep two black objects apart. The possibility of balanced, regular multi-black hole vacuum spacetimes can be motivated as follows. The five-dimensional vacuum Einstein's equations admit black ring solutions [8] which have horizons of topology $S^2 \times S^1$. Rotation prevents the black ring from collapsing. Very thin black rings are kept in equilibrium by a Newtonian force balance between a string-like tension and a centrifugal force arising from the rotation [9] (see also [10]). With this Newtonian balance in mind, it is natural to ask if rotation provides a sufficiently strong force to also keep a black ring in equilibrium in an "external potential". This could for instance be in the gravitational field of a Myers-Perry black hole [11] at the center of the black ring. Our solution realizes this possibility: a black ring balanced by rotation around a concentric spherical black hole in an asymptotically flat spacetime. We call this balanced configuration *black saturn*.

It should be emphasized that the black hole and the black ring generally have strong gravitational backreactions, so that only for very thin black rings with large S^1 radius does the motivation of a black ring in an external potential apply. On the other hand, the gravitational interactions between the two objects give rise to interesting phenomena, such as frame-dragging, which we examine in detail. We summarize here a selection of physical properties of black saturn:

- *Continuous non-uniqueness*: The total mass M and angular momentum J measured at infinity can be distributed continuously between the two black objects in the balanced saturn configuration. Thus the solution exhibits 2-fold continuous non-uniqueness. An additional discrete non-uniqueness exists in regimes that admit both thin and fat black rings.

- *Counter rotation*: The black ring and the S^3 black hole have independent rotation parameters, and they can be co-rotating as well as counter-rotating while maintaining

JHEP05(2007)050

balance. (We define co- and counter-rotation in terms of the relative sign of the angular velocities.)

- *Non-uniqueness of the 4+1d Schwarzschild black hole*: Strikingly, the black ring and S^3 black hole can be counter-rotating to give zero total ADM angular momentum at infinity. This means that the 4+1-dimensional Schwarzschild-Tangherlini black hole is not the only asymptotically flat black hole solution with $J = 0$ at infinity; in fact the $J = 0$ black saturn configurations are 2-fold continuously non-unique.

  The existence of the $J = 0$ black saturn solutions does not contradict the uniqueness theorem [12] that the Schwarzschild black hole is the only static asymptotically flat vacuum black hole solution; the reason is simply that black saturn, while being stationary, is non-static.

  We also conclude that the slowly spinning Myers-Perry black hole is not unique; allowing for non-connected horizons one can get around the perturbative results of [13].

- *Rotational frame-dragging*: The gravitational interaction between the black ring and the S^3 black hole manifests itself in form of rotational frame-dragging. This is most cleanly illustrated when the intrinsic angular momentum (measured by the Komar integral) of the S^3 black hole is set to zero, $J^{\rm BH}_{\rm Komar} = 0$. The angular velocity $\Omega^{\rm BH}$, however, is not zero but follows the behavior of the angular velocity $\Omega^{\rm BR}$ of the black ring. We interpret this as frame-dragging: the rotating black ring drags the spacetime around with it, and in effect the black hole rotates too, despite having no intrinsic spin, $J^{\rm BH}_{\rm Komar} = 0$. It is exciting to have access to rotational frame-dragging in an exact solution.

- *Countering frame-dragging*: Counter-rotation makes it possible to tune the intrinsic rotation $J^{\rm BH}_{\rm Komar}$ of the S^3 black hole, so that it "cancels" the effect of dragging caused by the surrounding black ring. This gives a solution for which the angular velocity of the black hole vanishes: $\Omega^{\rm BH} = 0$ while $J^{\rm BH}_{\rm Komar} \neq 0$.

We have found no black saturn configurations ($J = 0$ or J nonzero) for which the total horizon area of the S^3 black hole and black ring exceeds the area $a^{\rm Schw}_{\rm H}$ of the static 4+1-dimensional Schwarzschild black hole of the same ADM mass,[1] however there are saturn configurations with total area arbitrarily close to $a^{\rm Schw}_{\rm H}$ for any value of J. The resulting phase diagram of 4+1-dimensional black holes is discussed in more detail in [14], where black saturn thermodynamics is also studied.

It is worth noting that for 4+1-dimensional asymptotically flat black hole spacetimes the continuous non-uniqueness will go much further than the 2-fold continuous non-uniqueness of the simple black saturn system presented here. An obvious generalization of our solutions includes multiple rings of saturn. As argued above, the total mass and

[1] This observation leads to the general expectation that for fixed mass the entropy of the d-dimensional Schwarzschild black hole serves as an upper bound on the total entropy in any stationary d-dimensional asymptotically flat balanced black hole vacuum spacetime.

JHEP05(2007)050

angular momentum can be distributed continuously between the n black objects in such a spacetime, subject to balance conditions, and the result is $2(n-1)$-fold continuous non-uniqueness. Including the second angular momentum gives doubly spinning multiple black saturns with $3(n-1)$-fold continuous non-uniqueness, also for the $J_1 = J_2 = 0$ configurations. If, as anticipated, the total area is bounded by $a_{\rm H}^{\rm Schw}$ for given total mass, each component of an n-black hole system will necessarily have smaller area as n increases.

Supersymmetric black hole solutions with one or more concentric balanced black rings around a rotating S^3 black hole were constructed by Gauntlett and Gutowski [15]. Being supersymmetric, the solutions are extremally charged and saturate the BPS bound of 4+1-dimensional supergravity with U(1) vector multiplets. For the supersymmetric solutions, it is not possible to observe dragging effects or counter-rotation, as we do for our non-supersymmetric vacuum solutions, because the supersymmetric solutions have vanishing angular velocities. The first order nature of the supersymmetry conditions [16, 17] makes the construction of multi-black hole solutions a fairly straightforward superposition of harmonic functions. For non-supersymmetric black holes we do not have this luxury, and instead we have to solve the full second order Einstein's equations.

The black saturn solution is found using the inverse scattering method. This solution generating method was first adapted to Einstein's equations by Belinsky and Zakharov [18, 19], and has been used extensively to generate four-dimensional vacuum solutions (see for instance [20] and references therein). Recently, the inverse scattering method, and closely related solution generating techniques, have been applied to generate five-dimensional rotating black hole vacuum solutions. The Myers-Perry black hole with two independent rotation parameters was constructed by a smart implementation of the inverse scattering method by Pomeransky [21]. Also, the unbalanced black ring with rotation on the S^2 was constructed [22, 23]; this solution was constructed independently in [24] without use of solution generating techniques. The original balanced S^1 rotating black ring [8] has also been constructed by these methods [25, 26]. Most recently, Pomeransky and Sen'kov have succeeded in constructing a doubly-spinning black ring solution [27] using the inverse scattering method (numerical results were also obtained recently [28]).

We briefly review relevant aspects of the inverse scattering method in section 2, where we also provide details of the construction of the black saturn solution. Section 3 contains an analysis of the solution, including computations of the physical parameters and the balance condition. The physics of the black saturn system is studied in section 4. Open questions are discussed in section 5.

2. Construction of the solution

We review in section 2.1 the inverse scattering method with focus on the Belinsky-Zakharov (BZ) n-soliton transformations [18, 19] (a detailed review can be found in the book [20]). In section 2.2 we discuss the seed solution and generate the black saturn solution by soliton transformations. The final result for the metric is presented in section 2.3.

JHEP05(2007)050

2.1 The inverse scattering method

The inverse scattering method can used as a solution generating method for stationary axisymmetric spacetimes. These are D-dimensional spacetimes with $D-2$ commuting Killing vector fields, one of which is time. The method allows construction of new solutions from known ones by means of purely algebraic manipulations.

We write the D-dimensional stationary axisymmetric spacetime as

$$ds^2 = G_{ab}\, dx^a dx^b + e^{2\nu}\left(d\rho^2 + dz^2\right) , \tag{2.1}$$

where $a, b = 1, \ldots, D-2$ and all compoments of the metric are functions of ρ and z only: $G_{ab} = G_{ab}(\rho, z)$ and $\nu = \nu(\rho, z)$. Without loss of generality the coordinates can be chosen such that

$$\det G = -\rho^2 . \tag{2.2}$$

Then Einstein's equations separate into two groups, one for the $(D-2) \times (D-2)$ matrix G,

$$\partial_\rho U + \partial_z V = 0 , \tag{2.3}$$

where

$$U = \rho\,(\partial_\rho G)\, G^{-1} , \qquad V = \rho\,(\partial_z G)\, G^{-1} , \tag{2.4}$$

and the other for the metric factor $e^{2\nu}$,

$$\partial_\rho \nu = \frac{1}{2}\left[-\frac{1}{\rho} + \frac{1}{4\rho}\mathrm{Tr}(U^2 - V^2)\right] , \qquad \partial_z \nu = \frac{1}{4\rho}\mathrm{Tr}(UV) . \tag{2.5}$$

The equations (2.5) for ν satisfy the integrability condition $\partial_\rho \partial_z \nu = \partial_z \partial_\rho \nu$ as a consequence of (2.3). Hence, once a solution $G_{ij}(\rho, z)$ to (2.3) is found, one can determine $\nu(\rho, z)$ by direct integration.

The matrix equations (2.2) and (2.3) form a completely integrable system, meaning that one can find a set of spectral equations (a "Lax pair" or "L-A pair") whose compatibility conditions are exactly (2.2) and (2.3). The spectral equations for (2.2) and (2.3) are

$$D_1\Psi = \frac{\rho V - \lambda U}{\lambda^2 + \rho^2}\Psi , \quad D_2\Psi = \frac{\rho U + \lambda V}{\lambda^2 + \rho^2}\Psi , \tag{2.6}$$

with commuting differential operators D_1 and D_2 given by

$$D_1 = \partial_z - \frac{2\lambda^2}{\lambda^2 + \rho^2}\partial_\lambda , \quad D_2 = \partial_\rho + \frac{2\lambda\rho}{\lambda^2 + \rho^2}\partial_\lambda , \tag{2.7}$$

The complex spectral parameter λ is independent of ρ and z, and the generating function $\Psi(\lambda, \rho, z)$ is a $(D-2) \times (D-2)$ matrix such that $\Psi(0, \rho, z) = G(\rho, z)$.

The linearity of (2.6) allows algebraic construction of new solutions from known solutions based on the "dressing method". Given a known "seed" solution G_0, one constructs

the corresponding matrices U_0 and V_0 in (2.4), and determines a generating matrix Ψ_0 which solves (2.6) with U_0 and V_0. Then one seeks a new solution of the form

$$\Psi = \chi\, \Psi_0 \,, \tag{2.8}$$

where $\chi = \chi(\lambda, \rho, z)$ is the dressing matrix. Inserting (2.8) into (2.6) now gives a set of equations for χ. The matrix χ is further constrained by requiring that the new metric $G = \Psi(\lambda = 0, \rho, z)$ is real and symmetric.

We are here interested in so-called "n-soliton" dressing matrices, which are characterized by having n simple poles in the complex λ-plane, and we further restrict to cases where the poles are located on the real axis; this determines the location of the poles to be [18 – 20]

$$\tilde{\mu}_k = \pm\sqrt{\rho^2 + (z - a_k)^2} - (z - a_k) \,, \tag{2.9}$$

where a_k are n real constants. We refer to the "+" pole as a soliton and denote it by μ_k, while the "−" pole is an anti-soliton denoted by $\bar{\mu}_k$. Note $\mu_k \bar{\mu}_k = -\rho^2$.

In addition to the n real constants a_k, an n-soliton transformation is determined by n arbitrary constant real $(D-2)$-component vectors $m_0^{(k)}$, which we shall refer to as the BZ vectors. The components of these vectors will be called BZ parameters. In our applications, the BZ vectors control the addition of angular momentum to a static seed solution.

Given a seed solution G_0, the n-soliton transformation yields a new solution G with components

$$G_{ab} = (G_0)_{ab} - \sum_{k,l=1}^{n} \frac{(G_0)_{ac}\, m_c^{(k)}\, (\Gamma^{-1})_{kl}\, m_d^{(l)}\, (G_0)_{db}}{\tilde{\mu}_k \tilde{\mu}_l} \,. \tag{2.10}$$

(Repeated spacetime indices $a, b, c, d = 1, \ldots, D-2$ are summed.) The components of the vectors $m^{(k)}$ are

$$m_a^{(k)} = m_{0b}^{(k)} \left[\Psi_0^{-1}(\tilde{\mu}_k, \rho, z)\right]_{ba} \,, \tag{2.11}$$

where Ψ_0 is the generating matrix which solves (2.6) with U_0 and V_0 determined by G_0 as in (2.4), and $m_{0b}^{(k)}$ are the BZ parameters.

The symmetric matrix Γ is defined as

$$\Gamma_{kl} = \frac{m_a^{(k)}\, (G_0)_{ab}\, m_b^{(l)}}{\rho^2 + \tilde{\mu}_k \tilde{\mu}_l} \,, \tag{2.12}$$

and the inverse Γ^{-1} of Γ appears in (2.10).

The new matrix G of (2.10) does not obey (2.2); instead, an n-soliton transformation gives

$$\det G = (-1)^n \rho^{2n} \left(\prod_{k=1}^{n} \tilde{\mu}_k^{-2}\right) \det G_0 \,, \tag{2.13}$$

with $\det G_0 = -\rho^2$. One can deal with this problem and obtain a physical solution $G^{(\mathrm{ph})}$ such that $\det G^{(\mathrm{ph})} = -\rho^2$, by multiplying G by a suitable factor of ρ and $\tilde{\mu}_k$'s. In four spacetime dimensions, this method of uniform renormalization works well and allows one to construct for instance (multi)Kerr-NUT solutions from just flat Minkowski space. In

higher dimensions, however, uniform renormalization typically leads to nakedly singular solutions.

One way around this problem is to restrict the soliton transformation to a 2×2 block of the seed solution and perform uniform renormalization on this block. This has been applied to reproduce black ring solutions with a single angular momentum [23, 26]. The drawback of this method is clearly that it can only produce solutions with rotation in at most a single plane. This would be sufficient for our purposes here, but we prefer to present the solution generating method in a more general setting so as to facilitate generalization of our black saturn solution to include angular momentum in two independent planes. We therefore follow the strategy of [21] which is applicable in any spacetime dimension and does not suffer from the above-mentioned limitations.

The idea is to note that the factor multiplying $\det G_0$ in (2.13) is independent of the BZ vectors $m_0^{(k)}$. Start with a diagonal seed solution $(G_0, e^{2\nu_0})$ and remove first solitons with trivial BZ parameters (so as to not introduce any off-diagonal components in the matrix G). Then add back the *same* solitons but now with general BZ parameters. The resulting solution G satisfies $\det G = -\rho^2$ by construction. Moreover, the metric factor $e^{2\nu}$ of the full solution can easily be obtained from the seed G_0 as [21]

$$e^{2\nu} = e^{2\nu_0} \, \frac{\det \Gamma_{kl}}{\det \Gamma^{(0)}_{kl}} \,, \tag{2.14}$$

where $\Gamma^{(0)}$ and Γ are constructed as in (2.12) using G_0 and G, respectively.

We now turn from the general discussion to the construction of the black saturn solution.

2.2 Seed and soliton transformation for black saturn

For the analysis of axisymmetric solutions we make use of the results of [29, 30]. We refer to these papers for general discussions of higher-dimensional Weyl solutions and the analysis of the corresponding rod configurations.

The rod configuration for the seed of black saturn is shown in figure 1. The thick solid black lines correspond to rod sources of uniform density $+1/2$, whereas the dashed line segment corresponds to a rod source of uniform negative density $-1/2$. The rods in the t direction correspond to black hole horizons. Note that for $a_1 = a_5$ the negative rod is eliminated and the solution describes a static black ring around an S^3 black hole. This is an unbalanced configuration with a conically singular membrane keeping the black ring and the S^3 black hole apart. The negative density rod is included in order to facilitate adding angular momentum to the black ring.

Using the techniques of [29] we construct the full 4+1-dimensional vacuum solution corresponding to the rod configuration in figure 1. We find

$$G_0 = \mathrm{diag}\left\{ -\frac{\mu_1\,\mu_3}{\mu_2\,\mu_4}, \frac{\rho^2\,\mu_4}{\mu_5\,\mu_3}, \frac{\mu_5\,\mu_2}{\mu_1} \right\} , \qquad \det G_0 = -\rho^2 \,. \tag{2.15}$$

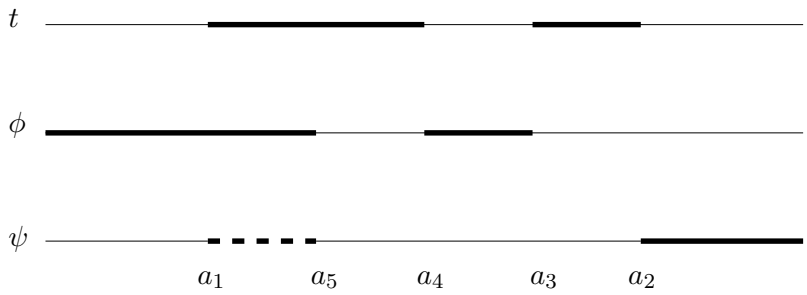

Figure 1: Sources for the seed metric G_0. The solid rods have positive density and the dashed rod has negative density. The rods are located at the z-axis with $\rho = 0$ and add up to an infinite rod with uniform density such that $\det G_0 = -\rho^2$. The labeling of the rod endpoints is a little untraditional, but is simply motivated by the fact that we are going to use the inverse scattering method to add solitons at $z = a_1$, a_2 and a_3.

The first term in G_0 corresponds to the tt-component, the second to the $\phi\phi$-component and the third to the $\psi\psi$-component. The μ_i are "solitons" as introduced in (2.9), i.e.

$$\mu_i = \sqrt{\rho^2 + (z - a_i)^2} - (z - a_i)\,, \tag{2.16}$$

where the a_i are the rod endpoints in figure 1. The metric factor $e^{2\nu}$ of the seed can written

$$e^{2\nu} = k^2\, \frac{\mu_2\,\mu_5(\rho^2+\mu_1\,\mu_2)^2(\rho^2+\mu_1\,\mu_4)(\rho^2+\mu_1\,\mu_5)(\rho^2+\mu_2\mu_3)(\rho^2+\mu_3\,\mu_4)^2(\rho^2+\mu_4\,\mu_5)}{\mu_1(\rho^2+\mu_3\mu_5)(\rho^2+\mu_1\,\mu_3)(\rho^2+\mu_2\,\mu_4)(\rho^2+\mu_2\,\mu_5)\prod_{i=1}^5(\rho^2+\mu_i^2)}\,. \tag{2.17}$$

The integration constant k will be fixed in section 3.3 for the full black saturn solution.

We assume the ordering

$$a_1 \le a_5 \le a_4 \le a_3 \le a_2 \tag{2.18}$$

of the rod endpoints.[2]

The solution (2.15) and (2.17) with the ordering (2.18) is singular and not in itself of physical interest. However, with a 1-soliton transformation we add an anti-soliton which mixes the t and ψ directions in such a way that the negative density rod moves to the t-direction and cancels the segment $[a_1, a_5]$ of the positive density rod. It turns out that this leaves a naked singularity at $z = a_1$, but choosing the BZ vector appropriately completely eliminates that singularity (see section 3.2). Taking $a_2 = a_3$ in the seed solution, this 1-soliton transformation gives the S^1 rotating black ring of [8]. We show this explicitly in appendix A.2.

Keeping $a_3 < a_2$, the above sketched 1-soliton transformation gives a rotating black ring around an S^3 black hole. This configuration can be balanced and we study its physical properties in detail in section 4.3. Including two more soliton transformations allow us to give the S^3 black hole independent rotation in two planes. The steps of generating the black saturn solution by a 3-soliton transformations are as follows:

[2]If instead we had chosen the different ordering $a_5 \le a_1 \le a_4 \le a_3 \le a_2$, then there would have been no negative density rod, and the solution (2.15) and (2.17) would describe two S^3 black holes and two conical singularities, one for each of the two finite rods in the angular directions. We will not use this ordering, but always take the rod endpoints to satisfy (2.18).

1. Perform the following three 1-soliton transformations on the seed solution (2.15):

   - Remove an anti-soliton at $z = a_1$ with trivial BZ vector (1,0,0); this is equivalent to dividing $(G_0)_{tt}$ by $-\rho^2/\bar{\mu}_1^2 = -\mu_1^2/\rho^2$.
   - Remove a soliton at $z = a_2$ with trivial BZ vector (1,0,0); this is equivalent to dividing $(G_0)_{tt}$ by $\left(-\rho^2/\mu_2^2\right)$.
   - Remove an anti-soliton at $z = a_3$ with trivial BZ vector (1,0,0); this is equivalent to dividing $(G_0)_{tt}$ by $-\rho^2/\bar{\mu}_3^2 = -\mu_3^2/\rho^2$.

   The result is the metric matrix

$$G_0' = \mathrm{diag}\left\{\frac{\rho^2\mu_2}{\mu_1\mu_3\mu_4}, \frac{\rho^2\mu_4}{\mu_3\mu_5}, \frac{\mu_2\mu_5}{\mu_1}\right\} . \tag{2.19}$$

2. Rescale G_0' by a factor of $\frac{\mu_1\mu_3}{\rho^2\mu_2}$ to find

$$\tilde{G}_0 = \frac{\mu_1\mu_3}{\rho^2\mu_2} G_0' = \mathrm{diag}\left\{\frac{1}{\mu_4}, \frac{\mu_1\mu_4}{\mu_2\mu_5}, -\frac{\mu_3}{\bar{\mu}_5}\right\} , \tag{2.20}$$

   where $\bar{\mu}_5 = -\rho^2/\mu_5$. This will be the seed for the next soliton transformation.

3. The generating matrix

$$\tilde{\Psi}_0(\lambda, \rho, z) = \mathrm{diag}\left\{\frac{1}{(\mu_4 - \lambda)}, \frac{(\mu_1 - \lambda)(\mu_4 - \lambda)}{(\mu_2 - \lambda)(\mu_5 - \lambda)}, -\frac{(\mu_3 - \lambda)}{(\bar{\mu}_5 - \lambda)}\right\} \tag{2.21}$$

   solves (2.6) with $\tilde{G}_0$. Note $\tilde{\Psi}(0, \rho, z) = \tilde{G}_0$.

4. Perform now a 3-soliton transformation with $\tilde{G}_0$ as seed:

   - Add an anti-soliton at $z = a_1$ (pole at $\lambda = \bar{\mu}_1$) with BZ vector $m_0^{(1)} = (1, 0, c_1)$,
   - Add a soliton at $z = a_2$ (pole at $\lambda = \mu_2$) with BZ vector $m_0^{(2)} = (1, 0, c_2)$, and
   - Add an anti-soliton at $z = a_3$ (pole at $\lambda = \bar{\mu}_3$) with BZ vector $m_0^{(3)} = (1, b_3, 0)$.

   Denote the resulting metric $\tilde{G}$. The constants c_1, c_2, and b_3 are the BZ parameters of the transformation.

5. Rescale $\tilde{G}$ to find

$$G = \frac{\rho^2\mu_2}{\mu_1\mu_3}\tilde{G} . \tag{2.22}$$

   This is needed to undo the rescaling of step 2, so that $\det G = -\rho^2$.

6. Construct $e^{2\nu}$ using (2.14). Note that Γ was found in the process of constructing G and that $\Gamma_0 = \Gamma\big|_{c_1=c_2=b_3=0}$. The result $(G, e^{2\nu})$ is the solution we want.

Some comments are in order. First, the rescaling in step 2 is simply a choice of convenience that yields a simple form for the generating matrix $\tilde{\Psi}_0$. Secondly, with $c_1 = c_2 = b_3 = 0$, the effect of the 3-soliton transformation in step 4 is simply to undo the transformation of step 1. Since (2.13) is independent of the BZ parameters c_1, c_2 and b_3, we are guaranteed to have $\det G = \det G_0 = -\rho^2$, after step 5 has undone the rescaling of step 2. Finally, in step 4 we could have added the (anti-)solitons with general BZ vectors $m_0^{(k)} = (a^{(k)}, b^{(k)}, c^{(k)})$ for $k = 1, 2, 3$. However, $b^{(k)} \neq 0$, $k = 1, 2$, or $c^{(3)} \neq 0$ lead to irremovable singularities and we therefore set $b^{(1)} = b^{(2)} = c^{(3)} = 0$. Finally, the solution is invariant under rescalings of the BZ vectors, $m_0^{(k)} \to \sigma_k\, m_0^{(k)}$ (no sum on k) for any nonzero σ_k, and we use the scaling freedom to set $a^{(k)} = 1$ without loss of generality.

In this paper we focus entirely on the black saturn solution with angular momentum only in a single plane, so we set $b_3 = 0$ in the following. The more general solution with $b_3 \neq 0$ remains to be analyzed.

2-soliton transformation

With $b_3 = 0$ the transformation described above is essentially a 2-soliton transformation. In fact, the saturn solution with $b_3 = 0$ can be produced by a 2-soliton transformation in much the same way as above. The resulting metric takes a slightly different form, but can be shown, using the explicit form of the μ_i's in (2.16), to be identical to the metric resulting from the 3-soliton transformation after a constant rescaling of the BZ parameters c_1 and c_2.

2.3 Saturn solution

The black saturn solution constructed by the above 3-soliton transformation with $b_3 = 0$ can be written[3]

$$ds^2 = -\frac{H_y}{H_x}\left[dt + \left(\frac{\omega_\psi}{H_y} + q\right) d\psi\right]^2 + H_x\left\{k^2\, P\Big(d\rho^2 + dz^2\Big) + \frac{G_y}{H_y}\, d\psi^2 + \frac{G_x}{H_x}\, d\phi^2\right\}. \quad (2.23)$$

For convenience we have chosen to write $e^{2\nu} = k^2\, H_x\, P$. Here k is the integration constant for the metric factor $e^{2\nu_0}$ given in (2.17), and $G_{x,y}$, $H_{x,y}$, and P are functions of ρ and z which will be given below. The constant q is included in order to ensure asymptotic flatness (we determine the value of q in the analysis of section 3.3).

With $b_3 = 0$, our soliton transformations leave the $\phi\phi$-part of the metric invariant, so from the static seed (2.15) we have

$$G_x = (G_0)_{\phi\phi} = \frac{\rho^2 \mu_4}{\mu_3\, \mu_5}\,. \quad (2.24)$$

The metric (2.23) involves the functions

$$P = (\mu_3\, \mu_4 + \rho^2)^2 (\mu_1\, \mu_5 + \rho^2)(\mu_4\, \mu_5 + \rho^2)\,, \quad (2.25)$$

[3]After performing the BZ transformation, we shift t as $t \to t - q\,\psi$ in order to ensure asymptotic flatness. At this point ψ is not assumed to be periodic so the shift does not effect the global structure of the solution. The periodicities of ψ and ϕ will be fixed in section 3. We have also reversed the sense of rotation by taking $\psi \to -\psi$.

and

$$H_x = F^{-1}\left[M_0 + c_1^2\, M_1 + c_2^2\, M_2 + c_1\, c_2\, M_3 + c_1^2 c_2^2\, M_4\right], \tag{2.26}$$

$$H_y = F^{-1}\,\frac{\mu_3}{\mu_4}\left[M_0\frac{\mu_1}{\mu_2} - c_1^2\, M_1\frac{\rho^2}{\mu_1\,\mu_2} - c_2^2\, M_2\frac{\mu_1\,\mu_2}{\rho^2} + c_1\, c_2\, M_3 + c_1^2 c_2^2\, M_4\frac{\mu_2}{\mu_1}\right], \tag{2.27}$$

where

$$M_0 = \mu_2\,\mu_5^2(\mu_1-\mu_3)^2(\mu_2-\mu_4)^2(\rho^2+\mu_1\,\mu_2)^2(\rho^2+\mu_1\,\mu_4)^2(\rho^2+\mu_2\,\mu_3)^2\,, \tag{2.28}$$

$$M_1 = \mu_1^2\,\mu_2\,\mu_3\,\mu_4\,\mu_5\,\rho^2\,(\mu_1-\mu_2)^2(\mu_2-\mu_4)^2(\mu_1-\mu_5)^2(\rho^2+\mu_2\,\mu_3)^2\,, \tag{2.29}$$

$$M_2 = \mu_2\,\mu_3\,\mu_4\,\mu_5\,\rho^2\,(\mu_1-\mu_2)^2(\mu_1-\mu_3)^2(\rho^2+\mu_1\,\mu_4)^2(\rho^2+\mu_2\,\mu_5)^2\,, \tag{2.30}$$

$$\begin{aligned} M_3 = {} & 2\mu_1\mu_2\,\mu_3\,\mu_4\,\mu_5\,(\mu_1-\mu_3)(\mu_1-\mu_5)(\mu_2-\mu_4)(\rho^2+\mu_1^2)(\rho^2+\mu_2^2) \\ & \times(\rho^2+\mu_1\,\mu_4)(\rho^2+\mu_2\,\mu_3)(\rho^2+\mu_2\,\mu_5)\,, \end{aligned} \tag{2.31}$$

$$M_4 = \mu_1^2\,\mu_2\,\mu_3^2\,\mu_4^2\,(\mu_1-\mu_5)^2(\rho^2+\mu_1\,\mu_2)^2(\rho^2+\mu_2\,\mu_5)^2\,, \tag{2.32}$$

and

$$\begin{aligned} F = {} & \mu_1\,\mu_5\,(\mu_1-\mu_3)^2(\mu_2-\mu_4)^2(\rho^2+\mu_1\,\mu_3)(\rho^2+\mu_2\,\mu_3)(\rho^2+\mu_1\,\mu_4) \\ & \times(\rho^2+\mu_2\,\mu_4)(\rho^2+\mu_2\,\mu_5)(\rho^2+\mu_3\,\mu_5)\prod_{i=1}^{5}(\rho^2+\mu_i^2)\,. \end{aligned} \tag{2.33}$$

Finally we have

$$G_y = \frac{\mu_3\,\mu_5}{\mu_4}\,, \tag{2.34}$$

and the off-diagonal part of the metric is given by

$$\omega_\psi = 2\frac{c_1\,R_1\sqrt{M_0M_1} - c_2\,R_2\sqrt{M_0M_2} + c_1^2\,c_2\,R_2\sqrt{M_1M_4} - c_1\,c_2^2\,R_1\sqrt{M_2M_4}}{F\sqrt{G_x}}\,. \tag{2.35}$$

Here $R_i = \sqrt{\rho^2+(z-a_i)^2}$.

Setting $c_1 = c_2 = 0$ gives $\omega_\psi = 0$ and $G_y H_x/H_y = \mu_2\,\mu_5/\mu_1 = (G_0)_{\psi\psi}$. The full solution can be seen to simply reduce to the seed solution (2.15) and (2.17) in this limit.

Taking $c_1 = 0$ and then setting $a_1 = a_5 = a_4$ we obtain the singly spinning Myers-Perry black hole, which was constructed similarly in [21]. For details, see appendix A.1. Taking instead $c_2 = 0$ and then setting $a_2 = a_3$ we obtain the S^1 spinning black ring of [8]. Appendix A.2 presents the explicit coordinate transformation from Weyl coordinates (ρ, z) to ring coordinates (x, y). The black ring was obtained in [25] and [26] with a different transformation which involved two solitons and started with a different seed metric. The 1-soliton transformation used here appears to be simpler.[4]

It is useful to note that the only effect of changing the signs of both BZ parameters c_1 and c_2, taking $(c_1, c_2) \to (-c_1, -c_2)$, is a change of sense of the overall direction of rotation, i.e. the only effect is $G_{t\psi} \to -G_{t\psi}$.

[4]We thank Roberto Emparan for sharing with us the idea of obtaining the S^1-spinning black ring by a 1-soliton transformation.

JHEP05(2007)050

The metric (2.23) is sufficiently complicated that it is difficult to check algebraically that the Einstein vacuum equations are solved. We have resorted to numerical methods in order to check the vanishing of all components of the Ricci tensor.

Next we present an analysis of the main properties of the black saturn solution.

3. Analysis

We introduce a convenient parameterization of the solution, and then analyze the rod structure. The BZ parameter c_1 will be fixed in order to eliminate the singularity left-over from the negative density rod of the seed solution. Next it is shown that the solution is asymptotically flat. Regularity is analyzed and the balance condition obtained by elimination of a conical singularity. We analyze the horizon structure, and compute a number of physical quantities for the solution: the ADM mass and angular momentum, as well as angular velocities, temperatures and horizon areas of the two black holes. We compute the Komar integrals for mass and angular momentum and obtain a Smarr relation. We study various limits of the solution, and we comment on the analysis of closed timelike curves (of which we find none).

3.1 Parameterization

The seed solution (2.15)-(2.17) contains five dimensionfull parameters, namely the rod endpoints a_i, $i = 1, \ldots, 5$. Since the whole rod configuration can be shifted along the z-axis without changing the solution, the description in terms of the a_i's is redundant; in addition to the ordering (2.18) and the directions of the rods as given in figure 1 we only need the lengths of the rods. It is useful to also take out the overall scale of the solution so that the seed solution is described in terms of three dimensionless parameters and an overall scale.

We choose the overall scale L to be[5]

$$L^2 = a_2 - a_1 \,, \tag{3.1}$$

and we introduce three dimensionless parameters κ_i as

$$\kappa_i = \frac{a_{i+2} - a_1}{L^2} \,, \qquad \text{for} \quad i = 1, 2, 3 \,. \tag{3.2}$$

As a consequence of the ordering (2.18), the κ_i's satisfy

$$0 \leq \kappa_3 \leq \kappa_2 < \kappa_1 \leq 1 \,. \tag{3.3}$$

(We exclude $\kappa_2 = \kappa_1$ for the balanced solution for reasons which will be apparent in section 3.4.) We shift and scale the z coordinate accordingly: set

$$z = L^2 \bar{z} + a_1 \,. \tag{3.4}$$

[5]The coordinates ρ and z, and hence the rod endpoints a_i, have dimensions (length)^2.

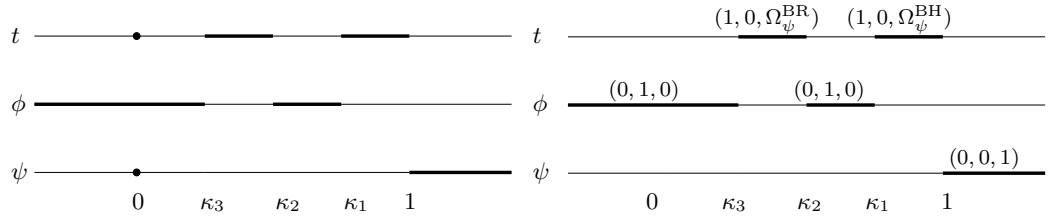

Figure 2(a) Figure 2(b)

Figure 2: Rod structure of the black saturn solution. Note that the rods are placed on the $\bar{z}$-axis, see section 3.2 for the definition of $\bar{z}$. The dots in figure 2(a) denote singularities at $\bar{z} = 0$, which are removed by the fixing c_1 according to (3.7) (figure 2(b)). This choice makes the $\rho = 0$ metric smooth across $\bar{z} = 0$. Figure 2(b) also shows the directions of the rods.

Then $\bar{z}$ is dimensionless. As we shall see in the following, the black ring horizon is located at $\rho = 0$ for $\bar{z} \in [\kappa_3, \kappa_2]$, and the S^3 black hole horizon at $\rho = 0$ for $\bar{z} \in [\kappa_1, 1]$.

The new parameterization effectively corresponds to taking

$$a_1 \to 0\,, \quad a_5 \to \kappa_3\,, \quad a_4 \to \kappa_2\,, \quad a_3 \to \kappa_1\,, \quad a_2 \to 1\,, \tag{3.5}$$

while carefully keeping track of the scale L.

The soliton transformations introduce the two dimensionfull BZ parameters, c_1 and c_2. It is convenient to redefine the BZ parameter c_2 by introducing the dimensionless parameter $\bar{c}_2$ as

$$\bar{c}_2 = \frac{c_2}{c_1(1-\kappa_2)}\,. \tag{3.6}$$

With this parameterization many expressions for the physical parameters simplify.

3.2 Rod structure

The rod structure at $\rho = 0$ is illustrated in figure 2. Harmark [30] introduces the "direction" of a given rod as the zero eigenvalue eigenvector of the metric matrix G at $\rho = 0$. The direction of each rod is indicated in figure 2(b). To summarize:

- The semi-infinite rod $\bar{z} \in]-\infty, \kappa_3]$ and the finite rod $[\kappa_2, \kappa_1]$ have directions $(0, 1, 0)$, i.e. they are sources for the $\phi\phi$-part of the metric.
- The semi-infinite rod $[1, \infty[$ has direction $(0, 0, 1)$, i.e. it is sourcing the $\psi\psi$-part of the metric.
- The finite rod $[\kappa_3, \kappa_2]$ corresponds to the location of the black ring horizon. It has direction $(1, 0, \Omega_\psi^{\rm BR})$. The finite rod $[\kappa_1, 1]$ corresponds to the location of the S^3 black hole horizon. It has direction $(1, 0, \Omega_\psi^{\rm BH})$. The angular velocities $\Omega_\psi^{\rm BR}$ and $\Omega_\psi^{\rm BH}$ will be given in section 3.5.

Note that the negative density rod of the seed solution figure 1 is no longer present. The soliton transformation which added the anti-soliton at $z = a_1$ has made the $+1/2$ and

$-1/2$ density rods in the t and ψ direction cancel. However, the cancellation of the rods left a singularity at $z = a_1$, i.e. $\bar{z} = 0$. This shows up as a $(z - a_1)^{-1} \sim \bar{z}^{-1}$ divergence in G_{tt} and $G_{\psi\psi}$, as indicated by dots in figure 2(a). Luckily, the singularities are removed completely by setting

$$|c_1| = L\sqrt{\frac{2\kappa_1\kappa_2}{\kappa_3}}\,. \tag{3.7}$$

With c_1 fixed according to (3.7), the metric at $\rho = 0$ is completely smooth across $\bar{z} = 0$. This means that we have succesfully removed the negative density rod at $\bar{z} \in [0, \kappa_3]$ ($z \in [a_1, a_5]$), and there is no longer any significance to the point $\bar{z} = 0$ ($z = a_1$) in the metric, as illustrated in figure 2(b).

The condition (3.7) will be imposed throughout the rest of the paper. Since $(c_1, c_2) \to (-c_1, -c_2)$ just changes the overall direction of rotation, we choose $c_1 > 0$ without loss of generality.

3.3 Asymptotics

We introduce asymptotic coordinates (r, θ)

$$\rho = \frac{1}{2}r^2 \sin 2\theta\,, \qquad z = \frac{1}{2}r^2 \cos 2\theta\,, \tag{3.8}$$

such that

$$d\rho^2 + dz^2 = r^2\,(dr^2 + r^2 d\theta^2)\,. \tag{3.9}$$

The asymptotic limit is $r^2 = 2\sqrt{\rho^2 + z^2} \to \infty$. Requiring that $G_{t\psi} \to 0$ when $r \to \infty$ determines the constant q in the metric (2.23) to be

$$q = L\,\sqrt{\frac{2\kappa_1\kappa_2}{\kappa_3}}\,\frac{\bar{c}_2}{1 + \kappa_2\,\bar{c}_2}\,. \tag{3.10}$$

We have used the definition (3.6) of $\bar{c}_2$ and imposed (3.7) for c_1.

To leading order, the asymptotic metric is

$$e^{2\nu} \;=\; k^2\Big[1 + \kappa_2\,\bar{c}_2\Big]^2\,\frac{1}{r^2} + \dots\,, \tag{3.11}$$

which motivates us to choose the constant k to be

$$k \;=\; \Big|1 + \kappa_2\,\bar{c}_2\Big|^{-1}\,. \tag{3.12}$$

We shall assume[6] that $\bar{c}_2 \neq -\kappa_2^{-1}$. The asymptotic metric then takes the form

$$ds^2 = -dt^2 + dr^2 + r^2\,d\theta^2 + r^2\sin^2\theta\,d\psi^2 + r^2\cos^2\theta\,d\phi^2\,. \tag{3.13}$$

Below we show that the angles ψ and ϕ have periodicities

$$\Delta\psi = \Delta\phi = 2\pi\,, \tag{3.14}$$

so that the solution indeed is asymptotically flat.

[6]The solution with $\bar{c}_2 = -\kappa_2^{-1}$ is nakedly singular. See sections 3.4 and 4.6 for further comments.

3.4 Regularity and balance

In order to avoid a conical singularity at the location of a rod, the period $\Delta\eta$ of a spacelike coordinate $\eta(=\psi,\phi)$ must be fixed as

$$\Delta\eta = 2\pi \lim_{\rho\to 0} \sqrt{\frac{\rho^2 e^{2\nu}}{g_{\eta\eta}}} \,. \tag{3.15}$$

Requiring regularity on the rod $\bar{z} \in [1,\infty]$ fixes the period of ψ to be $\Delta\psi = 2\pi$, and regularity on the rod $\bar{z} \in [-\infty, \kappa_3]$ determines $\Delta\phi = 2\pi$. We have used (3.7) and (3.12).[7] According to the discussion in the previous section this ensures asymptotic flatness of the solution.

Next we consider regularity as $\rho \to 0$ for the finite rod $\bar{z} \in [\kappa_2, \kappa_1]$. Eq. (3.15) gives

$$\Delta\phi = 2\pi \, \frac{\kappa_1 - \kappa_2}{\left|1+\kappa_2\,\bar{c}_2\right| \sqrt{\kappa_1(1-\kappa_2)(1-\kappa_3)(\kappa_1-\kappa_3)}} \,. \tag{3.16}$$

When no constraints other than (3.7) are imposed, the metric has a conical singular membrane in the plane of the ring, extending from the inner S^1 radius of the black ring to the horizon of the S^3 black hole.

We can avoid this conical singularity and balance the solution by requiring the right hand side of (3.16) to be equal to 2π. Solving for $\bar{c}_2$ this gives us the balancing, or equilibrium, condition for black saturn, i.e.

$$\bar{c}_2 = \frac{1}{\kappa_2}\left[\epsilon \frac{\kappa_1-\kappa_2}{\sqrt{\kappa_1(1-\kappa_2)(1-\kappa_3)(\kappa_1-\kappa_3)}} - 1\right] , \quad \text{with} \quad \begin{cases} \epsilon = +1 & \text{when} \;\; \bar{c}_2 > -\kappa_2^{-1} \\ \epsilon = -1 & \text{when} \;\; \bar{c}_2 < -\kappa_2^{-1} \end{cases} . \tag{3.17}$$

The solution with $\bar{c}_2 = -\kappa_2^{-1}$ is nakedly singular. Thus the choice of sign ϵ divides the balanced black saturn solutions into two separate sectors. The limit of removing the S^3 black hole to leave just the balanced black ring requires setting $\bar{c}_2 = 0$ and according to (3.17) this is only possible for $\epsilon = +1$. We are going to study the $\epsilon = +1$ solutions in detail in section 4, but will also discuss some properties of the $\epsilon = -1$ solutions (see sections 3.7 and 4.6).

3.5 Horizons

The rod analysis of section 3.2 showed that the two horizon rods had directions $(1, 0, \Omega^i_\psi)$, $i = \mathrm{BR}, \mathrm{BH}$, for the black ring and the S^3 black hole. Equivalently, the Killing vectors $\xi = \partial_t + \Omega^i_\psi \partial_\psi$ are null on the respective horizons. The angular velocities Ω^i_ψ are

$$\Omega^{\mathrm{BH}}_\psi = \frac{1}{L}\left[1+\kappa_2\,\bar{c}_2\right] \sqrt{\frac{\kappa_2\kappa_3}{2\kappa_1}} \, \frac{\kappa_3(1-\kappa_1) - \kappa_1(1-\kappa_2)(1-\kappa_3)\bar{c}_2}{\kappa_3(1-\kappa_1) + \kappa_1\kappa_2(1-\kappa_2)(1-\kappa_3)\bar{c}_2^2} \,, \tag{3.18}$$

$$\Omega^{\mathrm{BR}}_\psi = \frac{1}{L}\left[1+\kappa_2\,\bar{c}_2\right] \sqrt{\frac{\kappa_1\kappa_3}{2\kappa_2}} \, \frac{\kappa_3 - \kappa_2(1-\kappa_3)\bar{c}_2}{\kappa_3 - \kappa_3(\kappa_1-\kappa_2)\bar{c}_2 + \kappa_1\kappa_2(1-\kappa_3)\bar{c}_2^2} \,. \tag{3.19}$$

The black ring and the S^3 black hole generally have different angular velocities.

[7] If we had not imposed the condition (3.7), which removes the singularity at $\bar{z} = 0$, then (3.15) would have given $\Delta\phi = \frac{\pi}{L}\sqrt{\frac{2\kappa_3}{\kappa_1\kappa_2}}\, c_1$ for $\bar{z} \in [0, \kappa_3]$. Requiring $\Delta\phi = 2\pi$ is precisely the condition (3.7).

Myers-Perry black hole horizon geometry

One black hole horizon is located at $\rho = 0$ for $\kappa_1 \leq \bar{z} \leq 1$ and the metric on a spatial cross-section of the horizon can be written

$$ds^2_{\rm BH} = \frac{2L^2(\bar{z}-\kappa_1)(\bar{z}-\kappa_3)}{(\bar{z}-\kappa_2)}\, d\phi^2 + L^2 s^2_{\rm BH}\, g(\bar{z})(1-\bar{z})\, d\psi^2 + \frac{L^2\,(\bar{z}-\kappa_2) d\bar{z}^2}{(1-\bar{z})(\bar{z}-\kappa_1)(\bar{z}-\kappa_3) g(\bar{z})}, \quad (3.20)$$

where the constant $s_{\rm BH}$ is

$$s_{\rm BH} = \frac{\kappa_3(1-\kappa_1) + \kappa_1\kappa_2(1-\kappa_2)(1-\kappa_3)\bar{c}_2^2}{\kappa_3\sqrt{(1-\kappa_1)(1-\kappa_2)(1-\kappa_3)}\left[1+\kappa_2\bar{c}_2\right]^2}, \quad (3.21)$$

and the function $g(\bar{z})$ is

$$\begin{aligned} g(\bar{z}) \,=\, & 2\kappa_1\kappa_3(1-\kappa_1)(1-\kappa_2)(1-\kappa_3)(\bar{z}-\kappa_2) \\ & \times\left[1+\kappa_2\bar{c}_2\right]^2\Big[(1-\kappa_1)^2\kappa_3\Big[\kappa_1(\bar{z}-\kappa_2) - \kappa_3\Big(\kappa_1 - \kappa_2(1-\bar{z})^2 - \kappa_1\kappa_2(2-\bar{z})\Big)\Big] \\ & \quad + 2\kappa_1\kappa_2\kappa_3(1-\kappa_1)(1-\kappa_2)(1-\kappa_3)(1-\bar{z})(\bar{z}-\kappa_1)\,\bar{c}_2 \\ & \quad + \kappa_1^2\kappa_2(1-\kappa_2)^2(1-\kappa_3)^2\,\bar{z}\,(\bar{z}-\kappa_1)\,\bar{c}_2^2\Big]^{-1}. \end{aligned} \quad (3.22)$$

Note that $s_{\rm BH} \geq 0$. One can check that $g(\bar{z})$ is positive for $\kappa_1 \leq \bar{z} \leq 1$, so for $s_{\rm BH} > 0$, the horizon is topologically an S^3. Metrically the S^3 is distorted by rotation, as is the case for a Myers-Perry black hole, and here the horizon is further deformed by the presence of the black ring.

Black ring horizon geometry

The black ring horizon is located at $\rho = 0$ for $\kappa_3 \leq \bar{z} \leq \kappa_2$. The metric of a spatial cross section of the horizon can be written

$$ds^2_{\rm BR} = \frac{2L^2(\kappa_2-\bar{z})(\bar{z}-\kappa_3)}{(\kappa_1-\bar{z})}\, d\phi^2 + L^2 s^2_{\rm BR}\, f(\bar{z})(\kappa_1-\bar{z})\, d\psi^2 + \frac{L^2 d\bar{z}^2}{(\kappa_2-\bar{z})(\bar{z}-\kappa_3) f(\bar{z})} \quad (3.23)$$

where the constant $s_{\rm BR}$ is

$$s_{\rm BR} = \sqrt{\frac{\kappa_2-\kappa_3}{\kappa_1(\kappa_1-\kappa_3)(1-\kappa_3)}}\, \frac{\left(\kappa_3 - \kappa_3(\kappa_1-\kappa_2)\bar{c}_2 + \kappa_1\kappa_2(1-\kappa_3)\bar{c}_2^2\right)}{\kappa_3\left[1+\kappa_2\bar{c}_2\right]^2}, \quad (3.24)$$

and the function $f(\bar{z})$ is

$$\begin{aligned} f(\bar{z}) \,=\, & 2\kappa_1\kappa_3(\kappa_1-\kappa_3)(1-\kappa_3)(1-\bar{z}) \\ & \times\left[1+\kappa_2\bar{c}_2\right]^2(\kappa_2-\kappa_3)^{-1}\Big[\kappa_3\Big[\kappa_2(\kappa_1-\bar{z}) + \kappa_3\Big(\kappa_2\big(1-\kappa_1(2-\bar{z})\big) - \kappa_1(1-\bar{z})^2\Big)\Big] \\ & \quad + 2\kappa_1\kappa_2\kappa_3(1-\kappa_3)(1-\bar{z})(\kappa_2-\bar{z})\bar{c}_2 \\ & \quad + \kappa_1\kappa_2^2(1-\kappa_3)^2\bar{z}(\kappa_2-\bar{z})\bar{c}_2^2\Big]^{-1}. \end{aligned} \quad (3.25)$$

It follows from (3.3) that $s_{\rm BR} \geq 0$, and it can be checked that $f(\bar{z})$ is positive for $\kappa_3 \leq \bar{z} \leq \kappa_2$. The coordinate ψ parametrizes a circle whose radius depends on $\bar{z}$. The coordinates

$(\bar{z}, \phi)$ parameterize a deformed two-sphere. The topology of the horizon is therefore $S^1 \times S^2$. As is the case for the black ring [8, 9], the metric of the horizon is not a direct product of the $S^1 \times S^2$ (contrary to the supersymmetric case [31 – 33, 15]). For black saturn the black ring horizon is further distorted by the presence of the S^3 black hole.

Horizon areas

It is straightforward to compute the horizon areas. We find

$$\mathcal{A}_{\rm BH} = 4L^3\pi^2 \sqrt{\frac{2(1-\kappa_1)^3}{(1-\kappa_2)(1-\kappa_3)}}\, \frac{1+\frac{\kappa_1\kappa_2(1-\kappa_2)(1-\kappa_3)}{\kappa_3(1-\kappa_1)}\,\bar{c}_2^2}{\big(1+\kappa_2\,\bar{c}_2\big)^2}\,, \tag{3.26}$$

$$\mathcal{A}_{\rm BR} = 4L^3\pi^2 \sqrt{\frac{2\kappa_2(\kappa_2-\kappa_3)^3}{\kappa_1(\kappa_1-\kappa_3)(1-\kappa_3)}}\, \frac{1-(\kappa_1-\kappa_2)\bar{c}_2+\frac{\kappa_1\kappa_2(1-\kappa_3)}{\kappa_3}\,\bar{c}_2^2}{\big(1+\kappa_2\,\bar{c}_2\big)^2}\,. \tag{3.27}$$

Note that for all real $\bar{c}_2$ and $0 < \kappa_3 < \kappa_2 < \kappa_1 < 1$, the expressions for the horizon areas are real and positive, hence well-defined. In particular, there are no signs of closed timelike curves.

Temperatures

We compute the temperatures using [30] and find

$$T_{\rm H}^{\rm BH} = \frac{1}{2L\,\pi}\sqrt{\frac{(1-\kappa_2)(1-\kappa_3)}{2(1-\kappa_1)}}\, \frac{\big(1+\kappa_2\,\bar{c}_2\big)^2}{1+\frac{\kappa_1\kappa_2(1-\kappa_2)(1-\kappa_3)}{\kappa_3(1-\kappa_1)}\,\bar{c}_2^2}\,, \tag{3.28}$$

$$T_{\rm H}^{\rm BR} = \frac{1}{2L\,\pi}\sqrt{\frac{\kappa_1(1-\kappa_3)(\kappa_1-\kappa_3)}{2\kappa_2(\kappa_2-\kappa_3)}}\, \frac{\big(1+\kappa_2\,\bar{c}_2\big)^2}{1-(\kappa_1-\kappa_2)\bar{c}_2+\frac{\kappa_1\kappa_2(1-\kappa_3)}{\kappa_3}\,\bar{c}_2^2}\,.$$

The ordering (3.3) ensures that the temperatures are non-negative.

The expressions for the temperatures are complimentary to those for the horizon areas (3.26)-(3.27): with the entropy being one quarter times the horizon area, $S = \mathcal{A}/(4G)$, we have two very simple expressions:

$$T_{\rm H}^{\rm BH} S^{\rm BH} = \frac{\pi}{2G}\,L^2(1-\kappa_1)\,, \qquad T_{\rm H}^{\rm BR} S^{\rm BR} = \frac{\pi}{2G}\,L^2(\kappa_2-\kappa_3)\,. \tag{3.29}$$

The former vanishes in the limit $\kappa_1 \to 1$ which gives an extremal rotating S^3 black hole. The latter vanishes when $\kappa_2 = \kappa_3$, which we interpret as the limit where the black ring becomes singular, as the $j = 1$ limit of the fat black rings.

3.6 ADM mass and angular momentum

The solution is asymptotically flat and it is straightforward to compute the ADM mass M and angular momentum J using the asymptotic coordinates introduced in section 3.3. We find

$$M = \frac{3\pi\,L^2}{4G}\,\frac{\kappa_3(1-\kappa_1+\kappa_2)-2\kappa_2\kappa_3(\kappa_1-\kappa_2)\bar{c}_2+\kappa_2\big[\kappa_1-\kappa_2\kappa_3(1+\kappa_1-\kappa_2)\big]\bar{c}_2^2}{\kappa_3\big[1+\kappa_2\bar{c}_2\big]^2} \tag{3.30}$$

and

$$J = \frac{\pi L^3}{G}\frac{1}{\kappa_3\big[1+\kappa_2\bar{c}_2\big]^3}\sqrt{\frac{\kappa_2}{2\kappa_1\kappa_3}}\Big[\kappa_3^2 - \bar{c}_2\kappa_3\Big[(\kappa_1-\kappa_2)(1-\kappa_1+\kappa_3)+\kappa_2(1-\kappa_3)\Big] \\ +\bar{c}_2^2\kappa_2\kappa_3\Big[(\kappa_1-\kappa_2)(\kappa_1-\kappa_3)+\kappa_1(1+\kappa_1-\kappa_2-\kappa_3)\Big] \\ -\bar{c}_2^3\kappa_1\kappa_2\Big[\kappa_1-\kappa_2\kappa_3(2+\kappa_1-\kappa_2-\kappa_3)\Big]\Big]\,. \tag{3.31}$$

It is worth noting that for any $\bar{c}_2 \in \mathbb{R}$ the ADM mass (3.30) is positive as a simple consequence of the ordering (3.3).

3.7 Komar integrals

Komar integrals evaluated on the horizon of each black hole allow us to compute a measure of the mass and angular momentum of the two objects of the saturn system.

Komar masses

In five spacetime dimensions, the Komar mass is given by

$$M_{\rm Komar} = \frac{3}{32\pi G}\int_S *d\xi\ , \tag{3.32}$$

where ξ is the dual 1-form associated to the asymptotic time translation Killing field ∂_t and S is the boundary of any spacelike hypersurface. Eq. (3.32) measures the mass contained in S, so the mass of each black hole in a multi-black hole spacetime is computed by taking S to be at the horizon H_i. Instead, if we take S to be the S^3 at infinity, then (3.32) gives the total mass of the system, which coincides with the ADM mass. In terms of the metric components we have

$$M^i_{\rm Komar} = \frac{3}{32\pi G}\int_{H_i} dz\, d\phi\, d\psi\ \frac{1}{\sqrt{-\det\, g}}\ g_{zz}g_{\phi\phi}\big[-g_{\psi\psi}\,\partial_\rho g_{tt}+g_{t\psi}\,\partial_\rho g_{t\psi}\big]\ , \tag{3.33}$$

which for the saturn solution gives

$$M^{\rm BH}_{\rm Komar} = \frac{3\pi L^2}{4G}\,\frac{\kappa_3(1-\kappa_1)+\kappa_1\kappa_2(1-\kappa_2)(1-\kappa_3)\,\bar{c}_2^2}{\kappa_3(1+\bar{c}_2\,\kappa_2)}\,, \tag{3.34}$$

$$M^{\rm BR}_{\rm Komar} = \frac{3\pi L^2}{4G}\,\frac{\kappa_2\big[1-(1-\kappa_2)\,\bar{c}_2\big]\big[\kappa_3-\kappa_3(\kappa_1-\kappa_2)\,\bar{c}_2+\kappa_1\kappa_2(1-\kappa_3)\,\bar{c}_2^2\big]}{\kappa_3(1+\bar{c}_2\,\kappa_2)^2}\,. \tag{3.35}$$

Note that (3.34)-(3.35) give

$$M_{\rm ADM} = M^{\rm BR}_{\rm Komar} + M^{\rm BH}_{\rm Komar}\ , \tag{3.36}$$

so the Komar masses add up to the ADM mass (3.30), even in the presence of the conical singularity. We discuss the sign of the Komar masses at the end of this subsection.

Komar angular momenta

The angular momentum Komar integral is given by

$$J_{\rm Komar} = \frac{1}{16\pi G}\int_S *d\zeta\ , \tag{3.37}$$

where ζ is the 1-form dual to the Killing field ∂_ψ, and S is the boundary of any space-like hypersurface. Now (3.37) measures the angular momentum contained within S, and therefore, if we choose S to be the horizons H_i, we can compute the "intrinsic" angular momentum of each black object. We have

$$J^i_{\rm Komar} = \frac{1}{16\pi G}\int_{H_i} dz\, d\phi\, d\psi\ \frac{1}{\sqrt{-\det\, g}}\ g_{zz}g_{\phi\phi}\big[-g_{\psi\psi}\,\partial_\rho g_{t\psi} + g_{t\psi}\,\partial_\rho g_{\psi\psi}\big]\ , \tag{3.38}$$

which gives

$$J^{\rm BH}_{\rm Komar} = -\frac{\pi L^3}{G}\sqrt{\frac{\kappa_1\kappa_2}{2\kappa_3}}\ \frac{\bar c_2\big[\kappa_3(1-\kappa_1)+\kappa_1\kappa_2(1-\kappa_2)(1-\kappa_3)\,\bar c_2^2\big]}{\kappa_3(1+\bar c_2\,\kappa_2)^2}\,, \tag{3.39}$$

$$\begin{aligned} J^{\rm BR}_{\rm Komar} = {}& \frac{\pi L^3}{G}\sqrt{\frac{\kappa_2}{2\kappa_1\kappa_3}} \\ & \times\frac{\big[\kappa_3-\kappa_2(\kappa_1-\kappa_3)\,\bar c_2+\kappa_1\kappa_2(1-\kappa_2)\,\bar c_2^2\big]\big[\kappa_3-\kappa_3(\kappa_1-\kappa_2)\,\bar c_2+\kappa_1\kappa_2(1-\kappa_3)\,\bar c_2^2\big]}{\kappa_3(1+\bar c_2\,\kappa_2)^3}\,. \end{aligned} \tag{3.40}$$

The Komar angular momenta add to up to $J_{\rm ADM}$ given in (3.31),

$$J_{\rm ADM} = J^{\rm BR}_{\rm Komar} + J^{\rm BH}_{\rm Komar}\ , \tag{3.41}$$

even without imposing the balance condition (3.17).

We shall refer to the Komar angular momentum as the "intrinsic" angular momentum of the black hole. Note that for $\bar c_2 = 0$, the S^3 black hole carries no intrinsic spin $J^{\rm BH}_{\rm Komar} = 0$. This was expected since the soliton transformation with $c_2 = 0$ did not add spin to the S^3 black hole directly.

Smarr relations

Black rings [8] and Myers-Perry black holes [11] satisfy the same Smarr formula

$$\frac{2}{3}M = T_{\rm H}S + J\,\Omega\,. \tag{3.42}$$

Using the expressions of the Komar masses (3.34)-(3.35) and the Komar angular momenta (3.39)-(3.40) we find that both the black ring and the black hole separately obey this Smarr relation:

$$\frac{2}{3}\,M^{\rm BR}_{\rm Komar} = T^{\rm BR}_{\rm H}S^{\rm BR} + \Omega^{\rm BR}_\psi J^{\rm BR}_{\rm Komar}\ , \qquad \frac{2}{3}\,M^{\rm BH}_{\rm Komar} = T^{\rm BH}_{\rm H}S^{\rm BH} + \Omega^{\rm BH}_\psi J^{\rm BH}_{\rm Komar}\ . \tag{3.43}$$

These Smarr relations are mathematical identities which relates the physical quantities measured at the horizon, and they can be derived quite generally for multi-black hole vacuum spacetimes [14]. The relations (3.43) hold without imposing the balance condition (3.17).

Sign of Komar masses

We have already noted that the total ADM mass (3.30) is always positive. Positivity of $M^{\rm BH}_{\rm Komar}$ in (3.34) requires that $\bar{c}_2 > -\kappa_2^{-1}$, and this selects the $\epsilon = +1$ case of the balance condition in section 3.4. Furthermore, imposing the balance condition (3.17) with $\epsilon = +1$ implies that $\bar{c}_2$ takes values $-\kappa_2^{-1} < \bar{c}_2 < (1-\kappa_2)^{-1}$, and thus both $M^{\rm BH}_{\rm Komar}$ in (3.34) and $M^{\rm BR}_{\rm Komar}$ in (3.35) are positive.

On the other hand, imposing the balance condition (3.17) with $\epsilon = -1$ means that $\bar{c}_2 < -\kappa_2^{-1}$, and — as can be seen from (3.34)-(3.35) — this gives $M^{\rm BH}_{\rm Komar} < 0$ while $M^{\rm BR}_{\rm Komar} > 0$.

One might take as a criterium for establishing the physical relevance of a multi-black hole system that each of the components in the system has positive mass. Clearly, at large separations the Komar mass of each object should agree with the positive ADM mass of the object, but that does not imply that the Komar masses in tightly bound gravitational systems need to be positive.[8] How, physically, can a solution with negative Komar mass occur?

It follows from the Smarr relation (3.43) that the Komar mass can be negative provided that the angular velocity Ω and Komar angular momentum $J_{\rm Komar}$ have opposite signs *and* that $\Omega J_{\rm Komar}$ is sufficiently large and negative to overwhelm the positive $T_{\rm H}S$-term. In black saturn, the physical mechanism behind opposite signs of $\Omega^{\rm BH}$ and $J^{\rm BH}_{\rm Komar}$ is rotational frame-dragging: the rotating black ring drags the S^3 black hole so that its horizon is spinning in the opposite direction of its "intrinsic" angular momentum. We examine this effect in detail in section 4.3. In that section we focus on solutions with $\bar{c}_2 = 0$, hence $\epsilon = +1$, and these have $J^{\rm BH}_{\rm Komar} = 0$; however, that analysis also serves to illustrate the physics which lies behind having $\Omega^{\rm BH} J^{\rm BH}_{\rm Komar} < 0$.

In conclusion, the solutions with $M^{\rm BH}_{\rm Komar} > 0$ ($\epsilon = +1$) and $M^{\rm BH}_{\rm Komar} < 0$ ($\epsilon = -1$) appear to be equally valid. We shall primarily focus on the $M^{\rm BH}_{\rm Komar} > 0$ solutions when we study the physics of black saturn in section 4, but we comment briefly on the $M^{\rm BH}_{\rm Komar} < 0$ solutions in section 4.6.

Finally, let us remark that single black hole spacetimes with counter-rotation (in the sense of $\Omega J < 0$) and negative Komar mass, but positive ADM mass, have been constructed numerically as solutions of five-dimensional Einstein-Maxwell theory with a Chern-Simons term [34]. In that case, part of the energy and angular momentum is carried by the electromagnetic fields making counter-rotation and negative Komar mass possible.

3.8 Closed timelike curves

One might expect the plane of the ring to be a natural place for closed timelike curves (CTCs) to appear, and we have focused our analysis on this region. For the case $\bar{c}_2 = 0$, we find analytically that $G_{\psi\psi} > 0$ for $\rho = 0$ and $z < \kappa_3$ (the plane outside the ring) and $\kappa_2 < z < \kappa_1$ (the plane between the ring and the black hole). So for $\bar{c}_2 = 0$ there are no CTCs in the plane of the ring (cf. [35]).

[8] We thank Roberto Emparan for discussions about this point, and also Harvey Reall for helpful comments.

When $\bar{c}_2 \neq 0$ the metric components are sufficiently complicated that we resort to numerical checks. We have performed such checks for examples where the S^3 black hole and the black ring are counter-rotating as well as co-rotating. Among other examples we have checked the counter-rotating cases with $J = 0$; no CTCs were found.

CTCs tend to appear when solutions are over-spinning, at least that is the case for supersymmetric black holes [36, 31 – 33, 15]. Hence we have checked in detail cases where the black hole and the ring are co-rotating and fast spinning. One such example is studied in section 4.4.2. For this 1-parameter family of solutions the S^3 black hole angular velocity covers a large range of co- and counter-rotation; we have checked numerically for CTCs in the plane of the ring and found none.

While we have found no signs of the appearance of closed timelike curves in our analysis, we emphasize that our numerical checks are not exhaustive. Rewriting the solution in ring coordinates (x, y) will probably be helpful for checking for CTCs.

3.9 Limits

Black saturn combines a singly spinning Myers-Perry spherical black hole with a black ring in a balanced configuration, and it is possible to obtain either of these solutions as limits of the balanced black saturn solution with $\epsilon = +1$. We describe here the appropriate limits, while details are relegated to the appendix.

Myers-Perry black hole limit

In the general solution, one can remove the black ring by first setting the BZ parameter $c_1 = 0$, thus eliminating the black ring spin, and then removing the black ring rod by taking $\kappa_2 = \kappa_3 = 0$. For the physical solution, where the singularity at $\bar{z} = 0$ has been removed, c_1 is fixed by (3.7) and we have to take the limit $\kappa_2, \kappa_3 \to 0$, in such a way that c_1 remains finite. This can be accomplished by first taking $\kappa_2 \to \kappa_3$ and then $\kappa_3 \to 0$. We provide details of this limit in appendix A.1.

Black ring limit

The black ring [8] is obtained by simply removing the S^3 black hole from the saturn configuration. This is done by first setting the angular momentum of the black hole to zero by taking $\bar{c}_2 = 0$, and then setting $\kappa_1 = 1$, which removes the S^3 black hole. We show in appendix A.2 that the remaining solution is exactly the black ring of [8] by rewriting the solution explicitly in ring coordinates x, y. The balance condition (3.17) becomes the familiar equilibrium condition for a single black ring.

No merger limit

It would be interesting if one could use the black saturn system to study a controlled merger of the S^3 black hole and the black ring. Unfortunately, this is not possible. Based on the rod configuration given in figure 2(b), the merger should correspond to merging the two horizon rods, $[\kappa_3, \kappa_2]$ of the black ring and $[\kappa_1, 1]$ of the S^3 black hole. Thus the merger would correspond to taking $\kappa_1 \to \kappa_2$. Imposing the balance condition (3.17), $\kappa_1 \to \kappa_2$ implies $\bar{c}_2 \to -\kappa_2^{-1}$. The solution with $\bar{c}_2 = -\kappa_2^{-1}$ is nakedly singular, and hence the

suggested merger limit is singular. As a side remark, we point out that the singular nature of the merger limit is in fact very similar to why two balanced Kaluza-Klein black holes held apart by a static bubble-of-nothing cannot be merged by taking a similar limit [37].

4. Physics of black saturn

We examine a selection of interesting physical properties of black saturn. In section 4.1 we establish that black saturn has 2-fold continuous non-uniqueness. Section 4.2 reviews basic properties of the Myers-Perry black hole and the black ring; properties which will be helpful for understanding the physics of black saturn.

It is useful to clarify notions of rotation and intrinsic spin:

- A black hole is rotating when its angular velocity Ω^i is nonzero.
- Co(counter)-rotation means $\Omega^{\rm BH}$ and $\Omega^{\rm BR}$ have the same (opposite) sign.
- We use the term *intrinsic* angular momentum to refer to the angular momentum $J_{\rm Komar}$ measured by the Komar integral evaluated at the horizon of the black hole.

The two black objects in black saturn interact gravitationally, and one effect is frame-dragging. This is cleanly illustrated for the case where the S^3 black hole has vanishing intrinsic angular momentum, $J^{\rm BH}_{\rm Komar} = 0$, but is nonetheless rotating, $\Omega^{\rm BH} \neq 0$. We found in section 3.7 that $J^{\rm BH}_{\rm Komar} = 0$ for $\bar{c}_2 = 0$, so in section 4.3 we study the $\bar{c}_2 = 0$ subfamily of black saturn configurations.

The general black saturn configurations with $\bar{c}_2 \neq 0$ are studied in sections 4.4 and 4.5. For $\bar{c}_2 \neq 0$ the S^3 black hole and the black ring have independent rotation parameters, and this makes it possible to have counter-rotating solutions and configurations with vanishing total angular momentum, $J = 0$. Having $\bar{c}_2 \neq 0$ is also necessary for realizing the full 2-fold continuous non-uniqueness.

Note that we are imposing the balance condition (3.4) with $\epsilon = +1$ throughout this section, with the exception of subsection 4.6.

4.1 Parameter counting and non-uniqueness

We begin by counting the parameters in the saturn solution. The full solution has six parameters: $\kappa_{1,2,3}$, satisfying $0 \leq \kappa_3 \leq \kappa_2 < \kappa_1 \leq 1$, one scale L, and the two BZ parameters c_1 and c_2. The parameter c_1 is fixed according to (3.7) in order to avoid a naked singularity at $\bar{z} = 0$. We conveniently rescaled c_2 to introduce the dimensionless parameter $\bar{c}_2 \propto c_2$ in (3.6). So the unbalanced solution has four dimensionless parameters, $\kappa_{1,2,3}$ and $\bar{c}_2$, and the scale L. The balance condition (3.17) imposes a constraint between $\bar{c}_2$ and $\kappa_{1,2,3}$, and in conclusion, the balanced black saturn solution has three dimensionless parameters and one scale L.

Fixing the ADM mass M of the full system fixes the scale L, and leaves three dimensionless parameters. Fixing further the only other conserved asymptotic quantity, namely the angular momentum J, leaves two free dimensionless parameters. Thus black saturn has 2-fold continuous non-uniqueness. We examine the non-uniqueness in greater detail in the following sections.

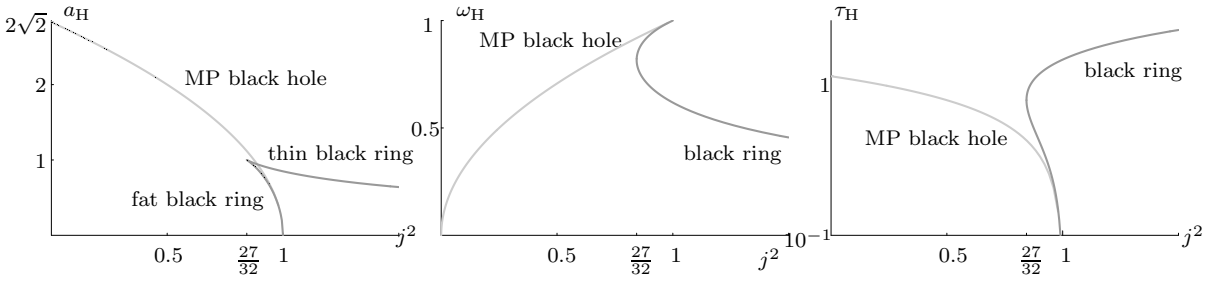

Figure 3(a) Figure 3(b) Figure 3(c)

Figure 3: Behavior of the reduced physical parameters for the Myers-Perry black hole (light gray) and the black ring (dark gray). Note that we are using a logarithmic scale for the temperature.

Fixed mass reduced parameters

We introduce the fixed mass reduced parameters

$$\begin{aligned} j^2 &= \frac{27\pi}{32G}\frac{J^2}{M^3}\,, & a_{\rm H}^i &= \frac{3}{16}\sqrt{\frac{3}{\pi}}\frac{\mathcal{A}_i}{(GM)^{3/2}}\,, \\ \omega_i &= \sqrt{\frac{8}{3\pi}}\,\Omega_\psi^i (GM)^{1/2}\,, & \tau_i &= \sqrt{\frac{32\pi}{3}}\,T_{\rm H}^i (GM)^{1/2}\,, \end{aligned} \tag{4.1}$$

which allow us to compare physical properties of configurations with the same ADM mass M. The script i labels the quantity corresponding to the black ring (i =BR) or the S^3 black hole (i=BH). We will also use the total horizon area,

$$a_{\rm H}^{\rm total} = a_{\rm H}^{\rm BR} + a_{\rm H}^{\rm BH}\,, \tag{4.2}$$

in order to study the "phase diagram" (total entropy vs. j^2) of the black saturn. Occasionally we simply use $a_{\rm H}$ for $a_{\rm H}^{\rm total}$.

The reduced temperature and angular velocity are normalized such that $\tau_{\rm BH} = 1$ for the five-dimensional Schwarzschild black hole ($j = 0$), and $\omega_{\rm BH} = 1$ for the maximally rotating (singular) Myers-Perry black hole ($j = 1$).[9]

4.2 Myers-Perry black hole and black rings

In preparation for studying the physical properties of black saturn, we review the basic properties of the Myers-Perry black hole [11] and the black ring [8] with a single angular momentum. Figure 3 shows for fixed mass the behaviors of the area, angular velocity and temperature of the Myers-Perry black hole and the black ring as the reduced angular momentum j is varied.

For the Myers-Perry black hole the reduced angular velocity grows linearly with the reduced angular momentum — in fact our normalization is such that $\omega_{\rm MP} = j_{\rm MP}$. (In order to better represent the near-$j = 1$ behavior we choose here to plot the physical properties vs. j^2 rather than j, as it was done in [9].) Increasing j, the area $a_{\rm H}^{\rm MP}$ decreases and the

[9]Our normalizations of τ_i and ω_i differ from the conventions used in [9].

black hole gets colder ($\tau_{\rm MP}$ decreases). As $j \to 1$, the S^3 horizon flattens out as a pancake in the plane of rotation, and at $j = 1$ the solution becomes nakedly singular.

Black rings come in two types: thin and fat black rings. The distinction is based on the "phase diagram" showing $a_{\rm H}^{\rm BR}$ vs. j^2 (see figure 3(a)): thin rings are those on the upper branch, while the fat rings are those on the lower branch. As $j \to 1$, the S^2 of fat rings flatten out in the plane of rotation, and the inner S^1 radius gets smaller while the outer S^1 radius grows (the shape of black rings was studied in detail in [9]). As j increases, the fat rings spin faster and become colder, much like the fast spinning Myers-Perry black hole. As $j \to 1$, the fat rings approach the same naked ring singularity of the $j = 1$ Myers-Perry solution.

A thin black ring has a nearly round S^2, and the S^1 radius is larger than the S^2 radius. As j increases, thin black rings get hotter as the S^2 gets smaller (and the ring thinner), and the angular velocity decreases. We shall see that many "phases" of black saturn also have versions of the "thin" and the "fat" black ring branches.

4.3 Configurations with $J^{\rm BH}_{\rm Komar} = 0$

Throughout this section we study the subfamily of black saturn with $\bar{c}_2 = 0$. It was shown in section 3.7 that for $\bar{c}_2 = 0$ the intrinsic angular momentum of the S^3 black hole vanishes, $J^{\rm BH}_{\rm Komar} = 0$.

When $\bar{c}_2 = 0$ it is simple to solve the balance condition (3.17) for κ_3: there are two solutions, but only one of them satisfies the constraints $0 < \kappa_3(\kappa_1, \kappa_2) < \kappa_2 < \kappa_1 < 1$. In order to illustrate the physics of the solution, we choose to further fix a physical quantity, so that we are left with a 1-parameter family of solutions. The extra physical parameter to be fixed will be either the reduced area of the black ring $a_{\rm H}^{\rm BR}$ (section 4.3.1) or the S^3 black hole $a_{\rm H}^{\rm BH}$ (section 4.3.2). Alternatively, we fix in section 4.3.3 the Komar mass of the black hole and test the gravitational interaction between the S^3 black hole and the black ring.

4.3.1 Fixed area black ring

As shown in figure 3(a), the reduced area $a_{\rm H}^{\rm BR}$ of a single black ring takes values $0 < a_{\rm H}^{\rm BR} \leq 1$. We can therefore fix the reduced black ring area at any value between 0 and 1 and then "grow" the S^3 black hole at the center of the black ring. The result is illustrated for representative values of $a_{\rm H}^{\rm BR}$ in figure 4.

For any value $0 < a_{\rm H}^{\rm BR} \leq 1$, there exist both a fat and a thin black ring, and the S^3 black hole can be grown from either. This is illustrated most clearly in figure 4(b), where we have fixed $a_{\rm H}^{\rm BR} = 0.8$ and plotted $a_{\rm H}^{\rm total}$ vs. j^2. The standard Myers-Perry black hole "phase" is shown in light gray, the black ring "phase" in darker gray. The black saturn configuration with fixed $a_{\rm H}^{\rm BR} = 0.8$ (black curve) starts at the thin and fat black ring branches at $a_{\rm H} = 0.8$. Since $J^{\rm BH}_{\rm Komar} = 0$, the S^3 black hole contributes no angular momentum, and hence j decreases as long as the black hole grows, i.e. until reaching the cusp of the curve in figure 4(b).

Figure 4(a) shows similarly the growth of an S^3 black hole at the center of the ring, but now with $a_{\rm H}^{\rm BR}$ fixed at smaller values, $a_{\rm H}^{\rm BR} = 0.1$ (dotted) and 0.05 (solid). The plot

JHEP05(2007)050

shows the saturn "phases" grow from the standard fat black ring branch; they meet the thin black ring branch at very large values of j not shown in figure 4(a). For such small fixed areas of the black ring, the S^3 black hole is allowed to grow very large, and these saturn "phases" dominate the standard black ring branch entropically.

Figures 4(c) and 4(d) show that the S^3 black hole is rotating, i.e. it has non-zero angular velocity $\omega_{\rm BH}$. That the S^3 black hole rotates despite carrying no intrinsic angular momentum ($J^{\rm BH}_{\rm Komar} = 0$) is naturally interpreted as gravitational frame-dragging: the rotating black ring drags the spacetime surrounding it and that causes the S^3 horizon to rotate. This interpretation is supported by the fact that the angular velocity $\omega_{\rm BH}$ follows, and is always smaller than, $\omega_{\rm BR}$.

To gain a better understanding of the physics of the black saturn, we first focus on the cases of small values of the fixed black ring area. The relevant plots are figure 4(a) ($a_{\rm H}^{\rm total}$ vs. j^2), figure 4(c) (angular velocities vs. j^2), and figure 4(e) (temperatures[10] vs. j^2) for fixed $a_{\rm H}^{\rm BR} = 0.1$ (dotted) and 0.05 (solid). For these values of the black ring area, the thin black ring is very thin, has large S^1 radius and is rotating slowly ($\omega_{\rm BR}$ is small). A small S^3 black hole at the center of such a thin black ring will hardly feel the surrounding ring. Indeed, for large j, the S^3 black hole has very small angular velocity $\omega_{\rm BH}$ (figure 4(c)), and it has large temperature $\tau_{\rm BH}$ (figure 4(e)) which decreases as the black hole grows. Thus the black hole behaves much like a small-mass Schwarzschild black hole, and we expect its horizon to be nearly round as long as it has small area.

Instead of growing the S^3 black hole from the thin black ring branch, consider starting with the fat black ring with $a_{\rm H}^{\rm BR} = 0.05$ or 0.1. The fat black ring has j near 1, the horizon is flattened out and it rotates fast. The S^3 black hole growing from this configuration will naturally be highly affected by the surrounding black ring. Consequently, the dragging-effect is much stronger, and indeed figure 4(c) shows that the S^3 black hole is rotating fast. Its temperature is very small (figure 4(e)), so it behaves much like the highly spinning small area Myers-Perry black hole near $j = 1$. Thus we expect the S^3 black hole to flatten out in the plane of the ring in this regime of black saturn.

Figures 4(b), 4(d), and 4(f) show the equivalent plots for the black ring area fixed at a larger value $a_{\rm H}^{\rm BR} = 0.8$. In this case, the distinction between growing the black hole from the thin or fat black ring branches is less pronounced. The S^3 black hole is always dragged along to that the angular velocity is far from zero, but even as the black ring becomes fat, the S^3 black hole never spins so fast that it enters the regime of the near-$j = 1$ Myers-Perry black hole as the area goes to zero. This effect can be seen from the temperature $\tau_{\rm BH}$ which increases as $a_{\rm H}^{\rm BH} \to 0$ — compare figures 4(e) and 4(f).

Increasing the fixed value of the black ring area, $a_{\rm H}^{\rm BR}$, the corresponding black saturn "phase" becomes smaller and smaller, and for fixed $a_{\rm H}^{\rm BR} = 1$ we find no saturn solutions. This is because growing the S^3 black hole with $J^{\rm BH}_{\rm Komar} = 0$ decreases the total angular momentum j, and for the black ring with $j = \sqrt{27/32}$ and $a_{\rm H}^{\rm BR} = 1$, there are no black ring solutions with less angular momentum.

[10]Note that we plot temperatures on a logarithmic scale in order to better capture the structure of all phases in one plot.

JHEP05(2007)050

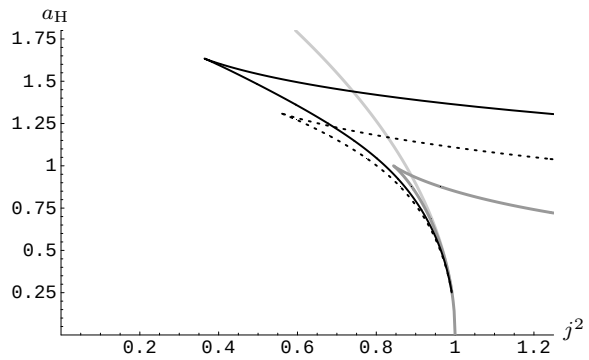

Figure 4(a): Total $a_{\rm H}$ for $a_{\rm H}^{\rm BR} = 0.05$ (solid) and $a_{\rm H}^{\rm BR} = 0.1$ (dotted).

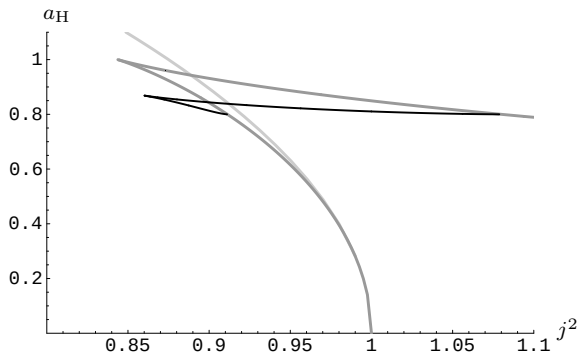

Figure 4(b): Total $a_{\rm H}$ for $a_{\rm H}^{\rm BR} = 0.8$.

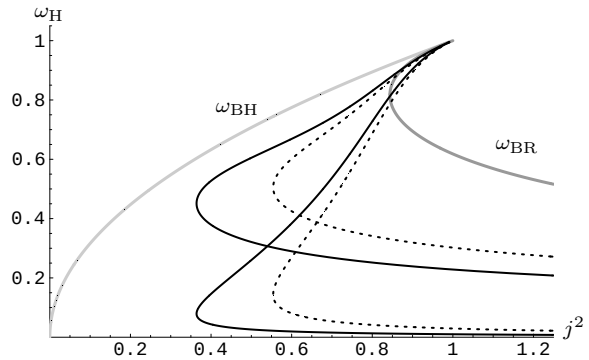

Figure 4(c): $\omega_{\rm BR}$ (upper curve) and $\omega_{\rm BH}$ (lower curve) for $a_{\rm H}^{\rm BR} = 0.05$ (solid) and $a_{\rm H}^{\rm BR} = 0.1$ (dotted).

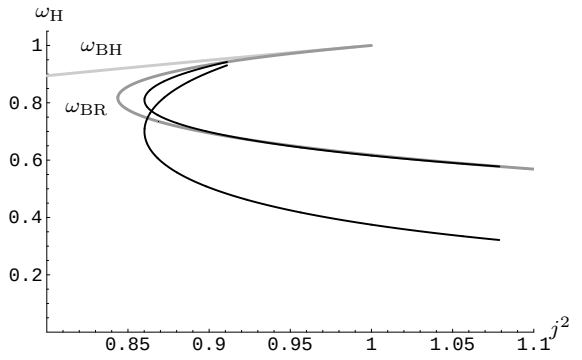

Figure 4(d): $\omega_{\rm BR}$ (upper curve) and $\omega_{\rm BH}$ (lower curve) for $a_{\rm H}^{\rm BR} = 0.8$.

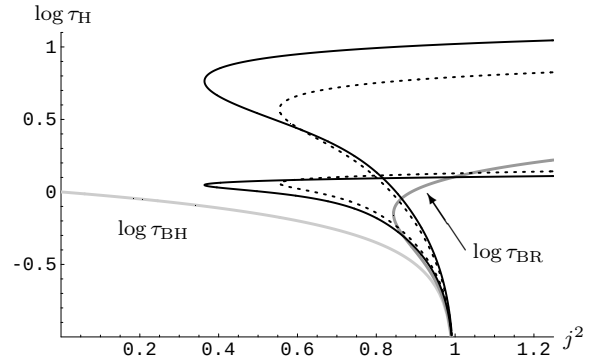

Figure 4(e): $\tau_{\rm BR}$ (lower curve) and $\tau_{\rm BH}$ (upper curve) for $a_{\rm H}^{\rm BR} = 0.05$ (solid) and $a_{\rm H}^{\rm BR} = 0.1$ (dotted).

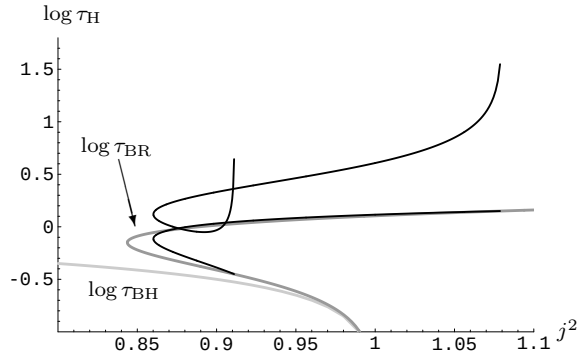

Figure 4(f): $\tau_{\rm BR}$ (lower curve) and $\tau_{\rm BH}$ (upper curve) for $a_{\rm H}^{\rm BR} = 0.8$.

Figure 4: For fixed total mass and some representative values of the $a_{\rm H}^{\rm BR}$, the various reduced quantities are plotted vs. j^2. The gray curves correspond to the Myers-Perry black hole (light gray) and the black ring (darker gray) respectively.

JHEP05(2007)050

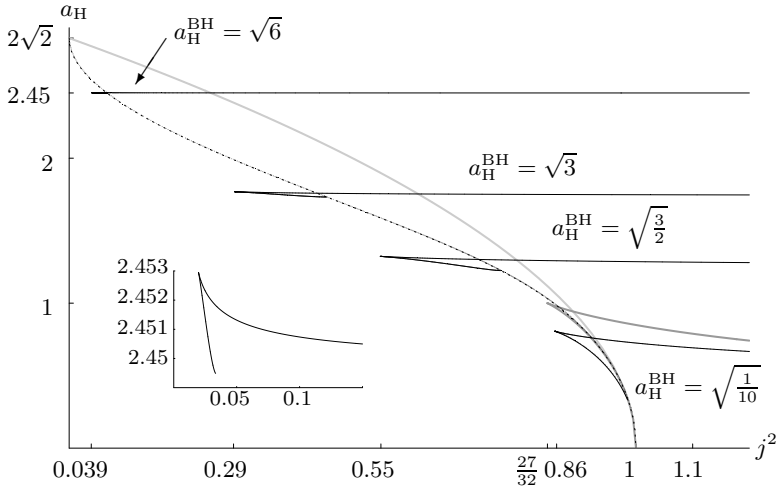

Figure 5: Plots of $a_{\rm H}$ vs. j^2 for different representative values of $(a_{\rm H}^{\rm BH})^2 = 6, 3, \frac{3}{2}, \frac{1}{10}$ (black solid curves). The dotted curve corresponds to a Myers-Perry black hole surrounded by a nakedly singular ring. Again, the gray curves correspond to the Myers-Perry hole (gray) and the black ring (darker gray). The smaller plot zooms in on the small j part of the $a_{\rm H}^{\rm BH} = \sqrt{6}$ curve.

Finally, let us note that it is possible to fix the black ring area to be zero, $a_{\rm H}^{\rm BR} = 0$. The $a_{\rm H}^{\rm BR} = 0$ saturn configuration describes a nakedly singular ring rotating around the S^3 black hole, which is also rotating as it is being dragged along by the ring singularity. The reduced area of the S^3 black hole vs. j^2 for this configuration is shown as a dotted curve in figure 5.

4.3.2 Fixed area black hole

We keep $\bar{c}_2 = 0$ as before, so that $J_{\rm Komar}^{\rm BH} = 0$, but instead of keeping the black ring area $a_{\rm H}^{\rm BR}$ fixed as in the previous subsection we now fix the S^3 black hole area $a_{\rm H}^{\rm BH}$. Thus we "grow" a black ring around the S^3 black hole area of fixed area. A balanced black ring cannot exist for arbitrarily small angular momentum while keeping the configuration in equilibrium, so the black ring grows from a nakedly singular ring around the Myers-Perry black hole; this is nothing but the $a_{\rm H}^{\rm BR} = 0$ configuration discussed at the end of the previous section, and shown as the dotted curve in figure 5.

Figure 5 shows black saturn phases with fixed black hole area for representative values of $a_{\rm H}^{\rm BH}$. For each value of $a_{\rm H}^{\rm BH}$, the corresponding curve has a fat and a thin black ring phase. Note that the thin ring branches extend to large values of j.

The large-j tails of the constant $a_{\rm H}^{\rm BH}$ curves show that balanced saturn configurations can have very large entropies. It can be argued [14] that for any fixed value of $0 < a_{\rm H}^{\rm BH} < 2\sqrt{2}$, the tails extend to arbitrarily large j. This in turn means that for any j there exist black saturn configurations with total area $a_{\rm H}^{\rm total}$ arbitrarily close to $2\sqrt{2}$. We refer to [14] for further details.

When the S^3 black hole area is close to zero, the black saturn curves approach the

phase of the single black ring. Since the black hole itself does not carry any intrinsic spin, we can set its area to zero, $a_{\rm H}^{\rm BH} = 0$, and then black saturn simply reduces to the black ring solution.

It is worth noting that for large values of $a_{\rm H}^{\rm BH}$, the black saturn curves also extend to small values of j. For $\bar{c}_2 = 0$, the saturn phases never reach $j = 0$. This is expected because $j = 0$ requires that the black hole and the black ring are counter-rotating and that is never the case for the $\bar{c}_2 = 0$.

4.3.3 Saturn frame-dragging

Above we have seen that in the presence of the rotating black ring of black saturn, an S^3 black hole with no intrinsic spin ($J_{\rm Komar}^{\rm BH} = 0$) can be rotating ($\omega_{\rm BH} \neq 0$). We have interpreted this as a consequence of gravitational frame-dragging. We test this interpretation by studying the geometry of the black saturn configuration (still keeping $\bar{c}_2 = 0$). If indeed we are seeing frame-dragging, then the effect should be very small when the black ring is thin and very far from the S^3 black hole, and increase as the black ring and the black hole come closer. We keep $m_{\rm BH} = M_{\rm Komar}^{\rm BH}/M$ fixed and let the distance between the black hole and black ring vary.

To characterize the configuration, we first introduce the reduced inner and outer S^1 (horizon) radii of the black ring

$$r_{\rm inner} = (GM)^{-1/2}\sqrt{G_{\psi\psi}}\Big|_{\rho=0,\,\bar{z}=\kappa_2}\,, \qquad r_{\rm outer} = (GM)^{-1/2}\sqrt{G_{\psi\psi}}\Big|_{\rho=0,\,\bar{z}=\kappa_3}\,. \tag{4.3}$$

It is shown in [9] that for a single black ring of fixed mass, the inner radius $r_{\rm inner}$ decreases monotonically when going from the thin black ring (i.e. large-j) regime to the fat black ring branch, and that $r_{\rm inner} \to 0$ when $j \to 1$ for the fat black rings. However, when a black hole is present at the center of the ring, as in black saturn, there is a lower bound on the inner radius of the black ring.[11]

Figure 6(a) shows the angular velocities of the S^3 black hole and the black ring plotted vs. $r_{\rm inner}$ for fixed Komar mass $m_{\rm BH} = 0.5$. The lower branch of the $\omega_{\rm BR}$ curve (black) corresponds to the slowly rotating "thin" black ring. For large radius, the S^3 black hole is not affected much and $\omega_{\rm BH}$ is correspondingly small (gray curve). As $r_{\rm inner}$ decreases the black ring spins faster and so does the S^3 black hole. Clearly there is a lower bound for $r_{\rm inner}$, but surprisingly, the ring starts growing after reaching this minimum. It turns out that on the "upper" branch of the $\omega_{\rm BR}$ curve, the inner and outer S^1 radii approach each other, so that the ring again becomes thin. But contrary to the standard thin black rings, the angular velocity increases as the ring grows. Eventually, as the black ring becomes thinner, the area $a_{\rm H}^{\rm BR}$ goes to zero leaving just a nakedly singular black ring around a Myers-Perry black hole (dotted curve in figure 5).

As shown in figure 6(a), the S^3 black hole angular velocity, $\omega_{\rm BH}$, follows that of the black ring. In particular, $\omega_{\rm BH}$ continues to grow even if the inner radius of the black ring is growing. This may at first seem to contradict that the rotation of the S^3 black hole is caused by frame-dragging, since it would seem that the S^3 black hole should slow down as

[11] As pointed out in section 3.9, there is no smooth merger limit for the balanced black saturn system.

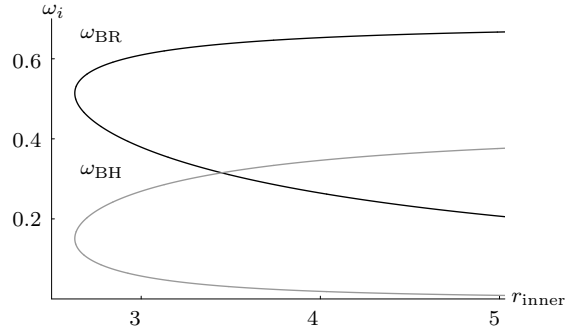

Figure 6(a)

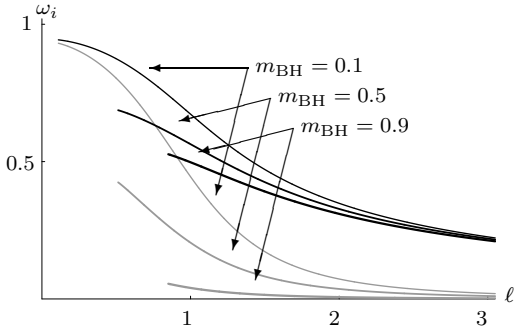

Figure 6(b)

Figure 6: Test of frame-dragging: figure 6(a) shows angular velocities ω_i vs. the inner radius of the black ring $r_{\rm inner}$ for fixed Komar mass $m_{\rm BH} = M^{\rm BH}_{\rm Komar}/M = 0.5$. Figure 6(b) shows the angular velocities ω_i vs. the proper distance ℓ between the black hole and the black ring for three different mass distributions: $m_{\rm BH} = M^{\rm BH}_{\rm Komar}/M = 0.1$, 0.5, and 0.9.

the black ring becomes thinner and its S^1 radius grows. However, since the S^3 black hole is itself rotating, it flattens out in the plane of rotation. To study this effect we compute the proper distance between the S^3 black hole and the black ring (for fixed mass):

$$\ell = (GM)^{-1/2} \int_{\kappa_2}^{\kappa_1} d\bar{z}\, \sqrt{G_{\bar{z}\bar{z}}}\,. \tag{4.4}$$

As expected, the proper distance ℓ increases as the inner radius of the black ring increases along the lower branch in figure 6(a). But even as the inner radius $r_{\rm inner}$ of the black ring increases (upper branch), the proper distance ℓ continues to decrease. This confirms that the black hole, as it is spinning faster, flattens out into the plane of rotation. Figure 6(b) shows the angular velocities as functions of the proper distance ℓ, for three different mass distributions $m_{\rm BH} = 0.1$, 0.5, and 0.9. The angular velocity of the black ring increases as the proper distance ℓ decreases. And $\omega_{\rm BH} \to 0$ when ℓ becomes large. This is precisely the behavior one would expect from frame-dragging.

Moreover, figure 6(b) shows that the effect of dragging depends on the relative masses of the black ring and the S^3 black hole: the effect of a thin small-mass black ring on a large-mass black hole is weak ($m_{\rm BH} = 0.9$), but the effect of a thick massive black ring on a small-mass black hole is strong ($m_{\rm BH} = 0.1$).

The above analysis gives strong evidence that we are indeed observing rotational frame-dragging.

4.4 Black hole with intrinsic spin

We now take $\bar{c}_2 \neq 0$ and study the more general saturn configurations. When $\bar{c}_2 \neq 0$, the S^3 black hole and the black ring have independent rotation parameters, in particular we can have $J^{\rm BH}_{\rm Komar} \neq 0$. As a result, the two black objects can be co- or counter-rotating. We illustrate the physics in two examples.

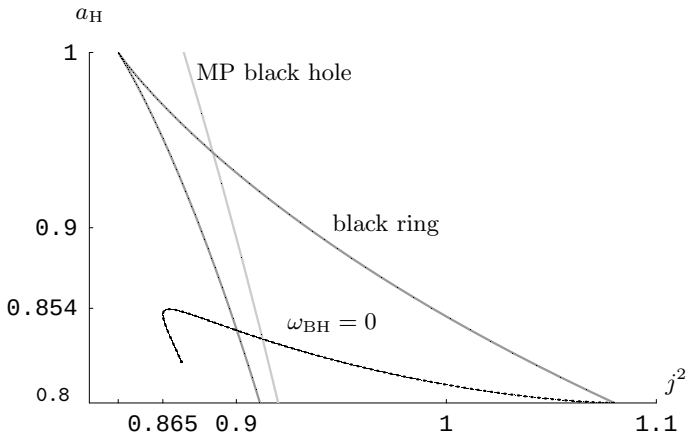

Figure 7: Black saturn with a non-spinning black hole. The plot shows $a_{\rm H}^{\rm total}$ vs. j^2 for fixed $a_{\rm H}^{\rm BR} = 0.8$ and $\omega_{\rm BH} = 0$ (dotted curve). For reference, the dark gray curve is the black ring while the lighter gray curve is the Myers-Perry black hole.

4.4.1 Counter-rotation and $\Omega_{\rm BH}$=0

In the previous section, the S^3 black hole had no intrinsic rotation, $J^{\rm BH}_{\rm Komar} = 0$, and it was rotating only because it was dragged along by the black ring. With $\bar{c}_2 \neq 0$ the S^3 black hole has its own intrinsic angular momentum $J^{\rm BH}_{\rm Komar} \neq 0$, and it is possible to let the S^3 black hole counter-rotate in such a way that the intrinsic angular momentum cancels the effect of the dragging, so that the S^3 horizon becomes non-rotating, $\omega_{\rm BH} = 0$.

As an example of this effect, figure 7 shows a curve of black saturn solution with $\omega_{\rm BH} = 0$ fixed. In addition we have also fixed $a_{\rm H}^{\rm BR} = 0.8$. This $\omega_{\rm BH} = 0$ curve starts at the thin black ring branch with $a_{\rm H} = 0.8$ and the black hole grows "Schwarzschild style" (zero angular velocity, high temperature which decreases as the black hole grows). As the black ring becomes fatter, the black hole is affected more and more by the ring, and at some point its intrinsic counter-rotation can no longer resist the dragging of the black ring; at this point the $\omega_{\rm BH} = 0$ curve ends.

The possibility of making the S^3 horizon non-rotating by turning on "intrinsic" angular momentum is reminiscent of the situation for the 4+1d supersymmetric S^3 black hole. This black hole also has a non-rotating horizon, $\Omega = 0$, and it can be shown [38] that this requires angular momentum to be stored in the Maxwell fields inside the horizon. Similar configurations were also discussed in [34]. Of course, for black saturn there are no Maxwell fields to carry the angular momentum, but the picture of having contributions to the rotation from "inside" the horizon to make $\omega_{\rm BH} = 0$ is common for the two systems.

4.4.2 Reaching $j = 0$

One might have expected the only solution with $j = 0$ to be the Schwarzschild black hole. However, taking into account solutions with more than one component of the horizon, counter-rotation can give $j = 0$. For black saturn this is possible while maintaining balance.

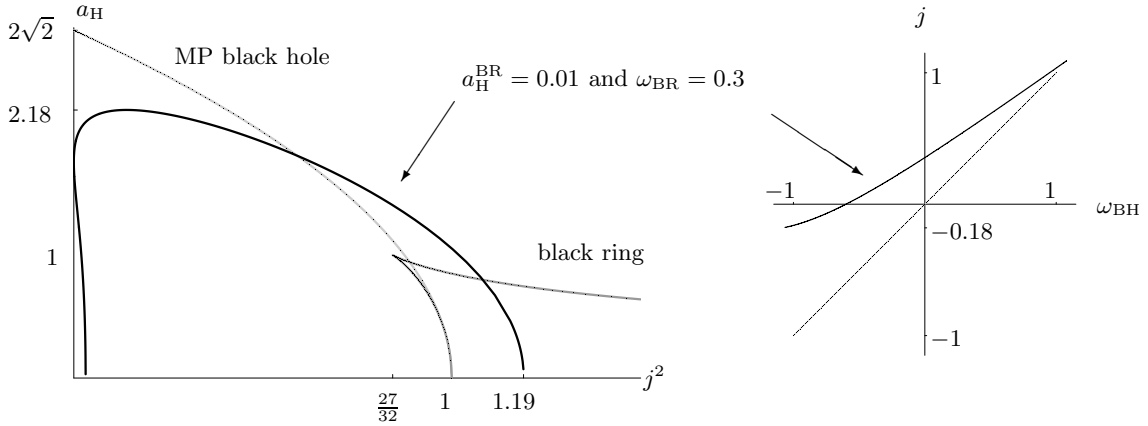

Figure 8: Left: Plot of a_H vs. j^2 for fixed $a_H^{BR} = 0.01$ and $\omega_{BR} = 0.3$ (black curve). Included are also the "phases" of a single Myers-Perry black hole (gray) and the black ring (darker gray). Right: j is plotted vs. the black hole for black saturn with $a_H^{BR} = 0.01$ and $\omega_{BR} = 0.3$ and for comparison with the corresponding curve for a single Myers-Perry black hole (light gray). The saturn configuration reaches $j = 0$ and extends to negative j.

Figure 8 shows a saturn configuration with $a_H^{BR} = 0.01$ and $\omega_{BR} = 0.3$ in the phase diagram a_H^{total} vs. j^2. To reach $j = 0$ requires that the black ring has small area, but otherwise there is nothing special about the values chosen for a_H^{BR} and ω_{BR}; they just illustrate the physics well. For large values j, the black ring and the S^3 black hole are co-rotating, as can be seen from the j vs. ω_{BH} plot in figure 8. As the angular velocity of the black hole decreases, the total angular momentum j decreases and the area of the S^3 black hole grows. The area reaches a maximum close to where the black hole angular velocity vanishes. As the S^3 black hole counter-rotates, $\omega_{BH} < 0$, the area decreases. Eventually, the counter-rotation is such that the total angular momentum at infinity vanishes, $j = 0$. The black hole can be even more counter-rotating and then j becomes negative. Note from the j vs. ω_{BH} plot in figure 8 that when the black holes are co-rotating j is almost linear in the angular momentum, just as it is for a Myers-Perry black hole, and the range covered $-1 \lesssim \omega_{BH} \lesssim 1$, is nearly the same.

It is clear from figure 8 that the 4+1d Schwarzschild black hole and the slowly spinning Myers-Perry black holes are not unique. We show in section 4.5.2 that there is a 2-fold continuous family of black saturn solutions with $j = 0$.

4.5 Non-uniqueness

In the previous sections we have examined a number of examples which — among other phenomena — all illustrated non-uniqueness in the phase diagram a_H vs. j^2. It is clear from these examples that black saturn covers large regions of the phase diagram. We now explore how large.

4.5.1 Non-uniqueness in the phase diagram

To study the region of the phase diagram covered by black saturn, we choose random sets of

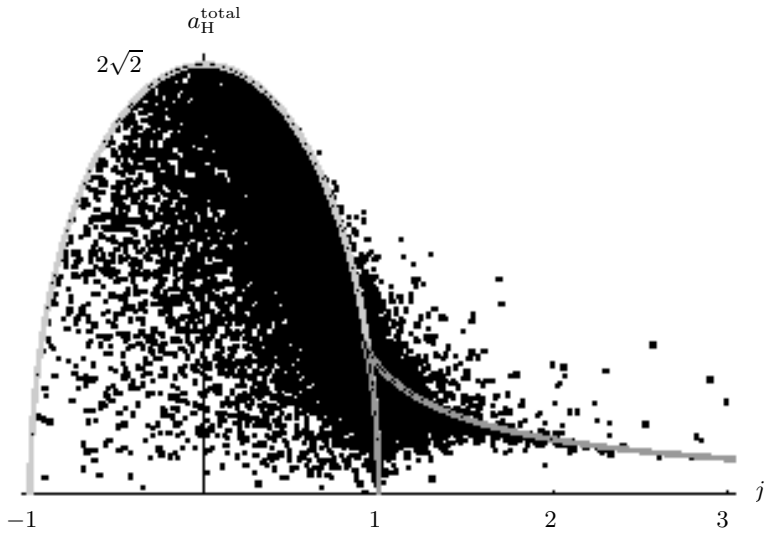

Figure 9: Non-uniqueness in the phase diagram: The plot shows the distribution of black saturn for 100.000 randomly chosen black saturn configurations.

points $(\kappa_1, \kappa_2, \kappa_3)$ satisfying the ordering (3.3) and plot the corresponding point $(j, a_{\rm H}^{\rm total})$ in the phase diagram.[12] Figure 9 shows the distribution of 100.000 such points.

We first note that we find no points with $j < -1$, thus black saturn takes values of $j \geq -1$. The asymmetry between positive and negative j is just a choice of rotation direction, which can be reversed by simply taking $\psi \to -\psi$ in the black saturn metric.[13]

Next the total area $a_{\rm H}^{\rm total}$ is always less than the area of the static Schwarzschild black hole, which has $a_{\rm H}^{\rm Schw} = 2\sqrt{2}$. We believe that there are black saturn configurations with $a_{\rm H}^{\rm total}$ arbitrarily close to $a_{\rm H}^{\rm Schw}$. In fact for the dataset shown, we have

$$\min(a_{\rm H}^{\rm Schw} - a_{\rm H}^{\rm total}) = 9.5 \cdot 10^{-4}\,. \tag{4.5}$$

The distribution[14] of black saturn configurations in the phase diagram figure 9 indicates that the region bounded by the Myers-Perry phase (shown in light gray for both positive and negative j) is fully covered by black saturn solutions. But there are also points outside this region: for j greater than ~ 0.5, there are black saturn solutions with total area greater than the Myers-Perry black hole and the black ring.

By tuning the distribution, it can be shown [14] that the whole open strip

$$0 < a_{\rm H}^{\rm total} < 2\sqrt{2} = a_{\rm H}^{\rm Schw}\,, \qquad j \geq 0\,, \tag{4.6}$$

is covered with black saturn configurations. For any $j \geq 0$ the high-entropy configurations are black saturn with an almost static S^3 black hole (accounting for the high entropy)

[12]The BZ parameter $\bar{c}_2$ is fixed in terms of $(\kappa_1, \kappa_2, \kappa_3)$ by the balance condition (3.17) with $\epsilon = +1$.

[13]It may also be noted that while $\omega_{\rm BH}$ takes both positive and negative values, we find that $\omega_{\rm BR}$ is always positive. The bound $\omega_{\rm BR} > 0$ is intuitively a consequence of the fact that the black ring needs to rotate in order to keep the system balanced.

[14]The density in the distribution is caused by the discrete non-uniqueness in regions where both thin and fat black rings exist, but can also be affected by the particular distribution of points $(\kappa_1, \kappa_2, \kappa_3)$.

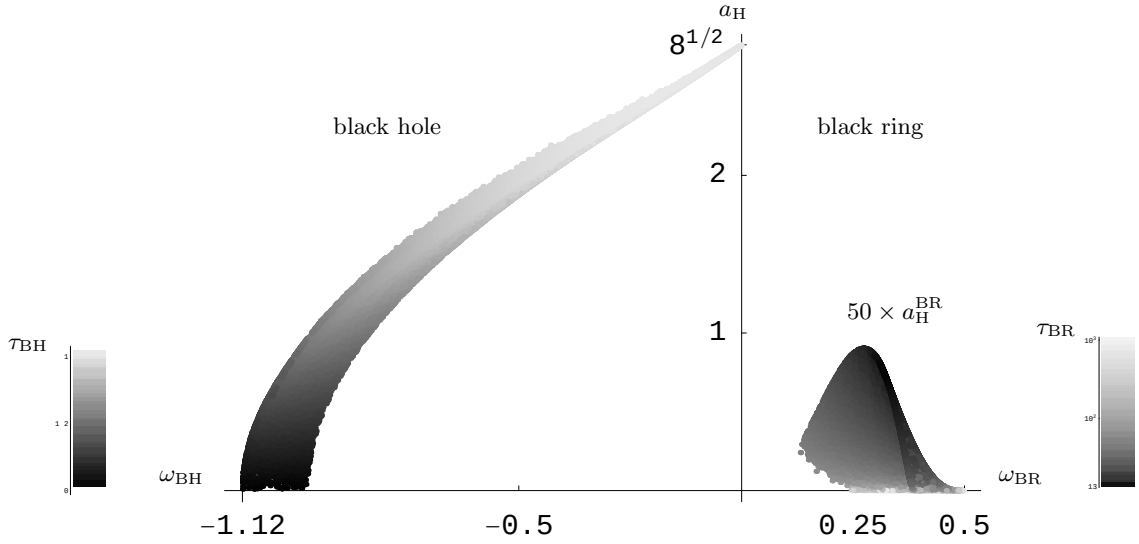

Figure 10: Non-uniqueness with $j = 0$: The plot shows the areas of the black hole (left) and black ring (right) vs. their respective angular velocities. Note that in order to fit the black hole and black ring areas on the same plot we have multiplied the black area by a factor of 50. The black holes are clearly counter-rotating. The points in the plots are colored according to the temperature. The black ring is always much hotter than the black hole, so different color scales are used for the black hole and the black ring.

surrounded by a large thin black ring (carrying the angular momentum). This type of configuration allow us to have black saturns with total area arbitrarily close to the bound set by the static Schwarzschild black hole. Details of this and the structure of the phase diagram are presented in [14].

4.5.2 Balanced saturn with zero angular momentum j=0

The phase diagram figure 9 strongly indicates that the $j = 0$ black saturn configurations are non-unique. We confirm the non-uniqueness in this section by studying the ranges of area, angular velocity and temperature covered by the balanced $j = 0$ saturn solutions.

Figure 10 shows the regions of the (ω_i, a_H^i) plane covered by the black ring and the S^3 black hole in saturn configurations with $j = 0$. Since $\omega_{BH} < 0$ and $\omega_{BR} > 0$, the two objects are clearly counter-rotating. Note that the black ring area a_H^{BR} has been multiplied by a factor of 50 in order for the plot be visible in the same plot as the S^3 black hole. The total area a_H^{total} never exceeds that of the 4+1d Schwarzschild black hole.

The points in figure 10 are colored according to the temperature τ_i of the corresponding black hole/ring: Light gray means hot and black means cold. The scales used for the black hole and the black ring temperatures are different, as shown in figure 10. The S^3 black hole temperature varies roughly between 0 and 3 (roughly like the Myers-Perry black hole which varies between 0 and 1), while the black ring is much hotter with temperature varying between 13 and $\sim 10^3$. This, and the very small area of the black ring, signals that these

JHEP05(2007)050

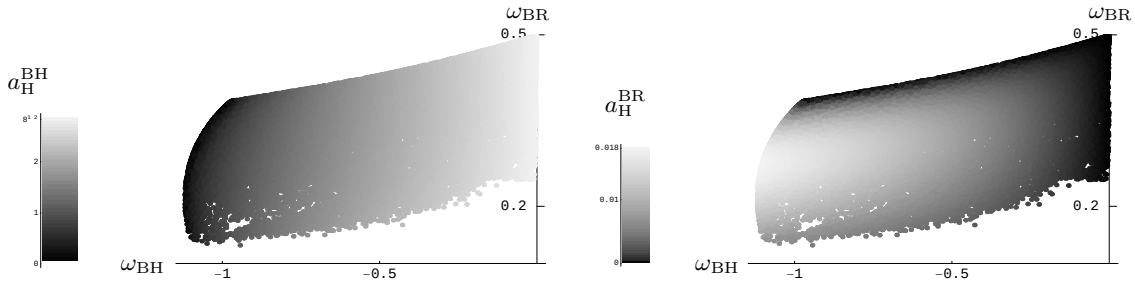

Figure 11: Non-uniqueness with $j = 0$: The two plots show the regions covered in "angular velocity space" when the angular momentum is fixed to zero, $j = 0$. Clearly the ring and the black hole are counter-rotating. On the left plot, the color shows the area of the black hole, while on the right plot it is the area of the black ring. Note again the scales are different and the black ring area is much smaller than that of the black hole.

are very thin, large radius black rings.

We further note that there is discrete non-uniqueness in the black ring sector of $j = 0$ black saturn. This can be seen by the "skirt" hanging over the righthand-part of the black ring area vs. $\omega_{\rm BR}$ "bell". The rings here have lower temperatures than the other rings with the same parameters, and it is therefore natural to interpret this "skirt" as a fat ring branch.

The points $(\omega_{\rm BH}, a_{\rm H}^{\rm BH})$ lie in the wedge shown in figure 10. For each point in this S^3 black hole wedge there is one (or two, in case of additional discrete non-uniqueness) corresponding point(s) in the black ring "bell". But it is not clear which S^3 black hole goes together with which black ring(s). That is illustrated better in figure 11, which shows two plots of $\omega_{\rm BR}$ vs. $\omega_{\rm BH}$. The first is colored according to the area of the black hole $a_{\rm H}^{\rm BH}$, while the second is colored according to the area of the black ring $a_{\rm H}^{\rm BR}$. Light gray means large area, black small area. As shown, different scales are used in the two plots.

In both figure 10 and figure 11 certain edges of the plots are rugged, and there are small white uncovered regions. This is simply due to the finite number of points generated for each plot, since some regions are covered less than others (this was also visible in figure 9).

4.5.3 Fixed j plots

We displayed in the previous section the regions of parameter space $(\omega_i, a_{\rm H}^i)$ covered by saturn configurations with $j = 0$. Likewise we can explore non-uniqueness for saturn configurations with j fixed at other values. Figure 12 shows $(\omega_i, a_{\rm H}^i)$ plots for representative values of fixed j.

When $j > \sqrt{27/32} \sim 0.92$, the S^3 black hole angular velocity $\omega_{\rm BH}$ and area $a_{\rm H}^{\rm BH}$ vary over a large range of values. This is shown in figures 12(a)-(d). As j becomes smaller than $j = \sqrt{27/32}$, which is the minimum value of j for the single black ring, the black ring of saturn has very small area and the range of the S^3 black hole parameters are more constrained, see figures 12(e)-(f). When the black ring and S^3 black hole are counter-rotating so that j is negative, the S^3 black hole parameters differ only little from the

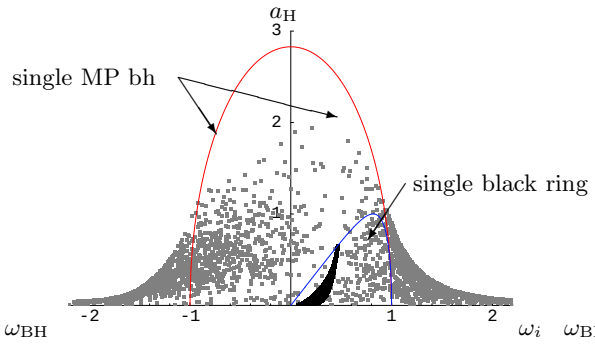

Figure 12(a): $j = 1.2$.

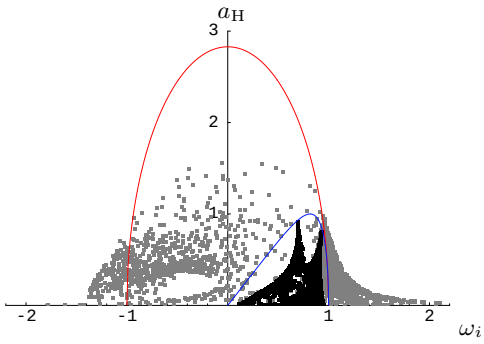

Figure 12(b): $j = 0.95$.

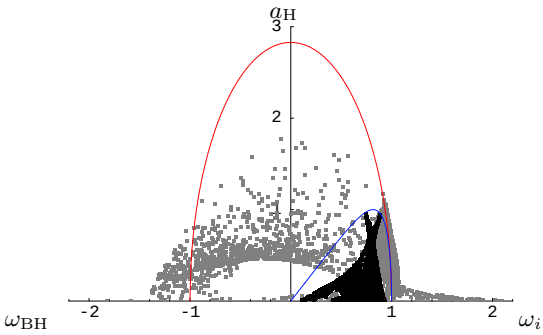

Figure 12(c): $j = 0.93$.

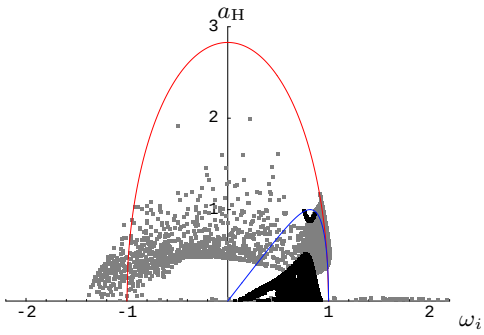

Figure 12(d): $j = 0.925$.

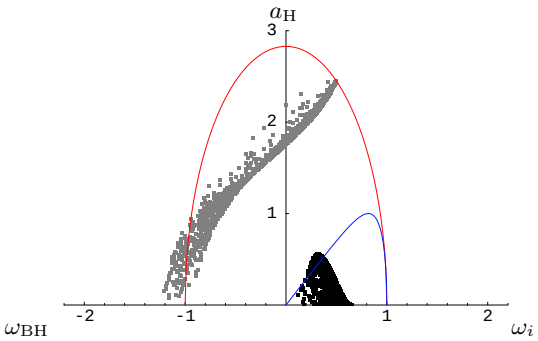

Figure 12(e): $j = 0.5$. The a_{BR} is multiplied by a factor of 10.

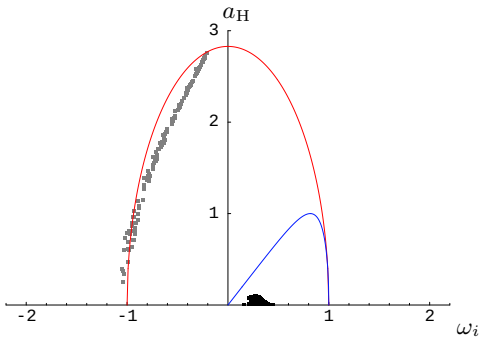

Figure 12(f): $j = 0.2$. The a_{BR} is multiplied by a factor of 10.

Figure 12: For fixed total mass and some representative values of j^2, the area of the black hole (gray dots) and the area of the black ring (black dots) are plotted against their respective angular velocities. The superimposed curves correspond to the area of a single Myers-Perry black hole against its angular velocity (upper curve), and similarly for the black ring. For these curves, the angular momentum j is of course not fixed. Note that for the black hole we included both the positive and negative ω_{BH}.

parameters of the Myers-Perry black hole, and the black ring is very thin and contributes little to the total area.

JHEP05(2007)050

4.6 Solutions with $\epsilon = -1$

Up to this point we have examined the physics of black saturn solutions for which the condition for balance (3.4) was imposed with the choice of sign $\epsilon = +1$, and hence $\bar{c}_2 > -\kappa_2^{-1}$. Here we briefly discuss the balanced saturn solutions with $\epsilon = -1$ for which $\bar{c}_2 < -\kappa_2^{-1}$.

As pointed out at the end of section 3.7, the solutions with $\bar{c}_2 > -\kappa_2^{-1}$ have positive Komar masses, while for $\bar{c}_2 < -\kappa_2^{-1}$, the Komar mass of the S^3 black hole is negative. We interpret this as an effect of extreme rotational frame-dragging, which makes $\Omega^{\rm BH} J^{\rm BH}_{\rm Komar}$ so negative that the Smarr relation (3.43) renders the Komar mass negative.

In the limit $\bar{c}_2 \to -\kappa_2^{-1}$, several of the dimensionful physical parameters diverge. However, the dimensionless fixed-mass reduced quantities remain finite. In particular, the dimensionless proper distance ℓ, defined in (4.4), between the black ring and the S^3 goes to zero when $\bar{c}_2 \to -\kappa_2^{-1}$. So this is a singular merger limit which ends in the nakedly singular $\bar{c}_2 = -\kappa_2^{-1}$ solution.

The balanced saturn solutions with $\bar{c}_2 < -\kappa_2^{-1}$ occupy only a small region of the phase diagram $(j, a_{\rm H}^{\rm total})$. They have $j \simeq -1$ and total area $0 < a_{\rm H}^{\rm total} \lesssim 1$. We interpret these solutions as tightly bound gravitational systems; they probably deserve a closer study than the one provided here.

5. Discussion

We have presented and analyzed a new exact solution to 4+1-dimensional vacuum Einstein equations describing Black Saturn: a Myers-Perry black hole surrounded by a black ring which is balanced by rotation in the plane of the ring. The system exhibits a number of interesting properties, such as non-uniqueness and frame-dragging, which were summarized in the Introduction.

Most surprising is probably the result that the 4+1-dimensional Schwarzschild black hole and slowly spinning Myers-Perry black holes are not unique. Black saturn shows that once multiple black hole horizons are considered (and staticity not assumed for the $J = 0$ configurations) black holes in 4+1-dimensions have large degeneracies. This and the structure of the phase diagram for 4+1-dimensional black holes can be found in [14].

We expect both black objects in black saturn to have ergoregions whenever their angular velocities are non-zero. This is always the case for the black ring, whose ergosurface is expected to have topology $S^1 \times S^2$ [8]. The S^3 black hole can be tuned to have zero angular velocity, and it is natural to expect that the solution, despite having non-vanishing intrinsic angular momentum, has no ergoregion. Generally, however, we expect an ergoregion bounded by an S^3 ergosurface. The metric in Weyl axisymmetric coordinates (ρ, z) is sufficiently complicated that we have not extracted useful equations for the ergoregions. We hope this will be addressed in future work, and note that it may be useful to first examine the $\rho = 0$ metric in order to examine the intersections of the ergosurfaces with the plane of the ring.

It would be desirable to transform the black saturn metric to a simpler coordinate system. The supersymmetric concentric black hole - black ring solutions of [15] can be

JHEP05(2007)050

written in ring coordinates (x, y) and it would presumably simplify our solution considerably to write it in such coordinates. We have presented in appendix A.2 the coordinate transformation from Weyl axisymmetric coordinates (ρ, z) to ring coordinates (x, y) for the simpler limit of the black ring without the S^3 black hole. We leave it to future work to convert the full black saturn solution to ring coordinates. We expect that ring coordinates will make it easier to study the ergoregions.

Focusing on the plane of the ring, we have numerically checked examples of co- and counter-rotating configurations, and found no closed timelike curves (CTCs). While we see no signs of CTCs — the horizon areas and temperatures are positive and well-defined in the full range of parameters — this should be analyzed in greater detail than done in this paper. Writing the solution in ring coordinates (x, y) will likely facilitate such an analysis.

The 1st law of thermodynamics for black saturn is studied in [14]. (We refer to refs. [39] and [40] for other works on black ring thermodynamics.) Black saturn is an example of an equilibrium system of two black objects which generally have different temperatures and different angular velocities. This is therefore only a classical equilibrium. It is shown in [14] that imposing thermodynamic equilibrium, in the sense of the two objects having equal temperatures and equal angular velocities, reduces the continuous family of saturns to a one-parameter family of equilibrium solutions with only discrete non-uniqueness. The phase diagram of equilibrium solutions is presented in [14].

The saturn system may well be classically unstable. The black ring of black saturn likely suffers from the same instabilities as the single black ring [8]. Using the Poincaré (or "turning-point") method, it was argued in [41] that (at least) one mode of instability would appear at the cusp of the black ring curve in the area vs. angular momentum phase diagram. At the cusp, where the thin and fat black ring branches meet, the black ring has minimum angular momentum and maximum entropy (for given mass). Studying the potential for the radial balance of a black ring, evidence was found [9] that a thin black ring would be stable under small radial perturbations while a fat black ring would be unstable. The radial instability of fat black rings appear exactly at the cusp, and so this mode is a physical concretization of the mode predicted by the turning-point method [41].[15]

Under radial perturbations, the analysis of [9] indicated that fat black rings either collapse to S^3 black hole (if perturbed inward) or possibly expand to become a thin black ring (if perturbed outwards). The latter may not happen in a dynamical process if thin black rings suffer from other classical instabilities, such as the Gregory-Laflamme instability [42], not captured by the turning-point method. Showing that Gregory-Laflamme modes always fit on (thin) black rings, refs. [10, 9] argued that thin black rings very likely suffer from Gregory-Laflamme instabilities. Likewise, we expect thin black rings of the black saturn system to be unstable to Gregory-Laflamme instabilities.

While some stability properties of black saturn can be expected to be inherited from the individual components, the Myers-Perry black hole and the single black ring, there

[15] Due to the continuous non-uniqueness, the implementation of the turning-point method for black saturn does not seem possible. Following [9] one can try to compute the radial potential for the black ring in black saturn, but here one also has to choose to fix some non-conserved quantities in order to carry out the analysis.

JHEP05(2007)050

can also be new instabilities for the black saturn system, for instance, perturbation of the center-of-mass of the S^3 black hole away from the center of the ring.

We constructed the black saturn solution using the inverse scattering method [18 – 20]. The seed solution and the soliton transformations invite a number of interesting generalizations of black saturn:

- *Multiple rings of saturn*: It is straightforward to generalize the seed solution to include more rod sources that will correspond to black ring horizons. One can also add negative density rods to facilitate the addition of angular momentum for each black ring using (anti)soliton transformations like we did in section 2.2. Provided all singularities can be removed as done here, and the system balanced, the generated solution will describe "the multiple rings of black saturn". One interesting property of multiple ring solutions is the high degree of continuous non-uniqueness as we discussed in the Introduction.

- *Doubly spinning black saturn*: The 3-soliton transformation in section 2.2 adds a second angular momentum for the S^3 black hole when $b_3 \neq 0$. An analysis of this solution is required to check that all possible singularities can be eliminated. Then it will be interesting to study the physics of this doubly spinning saturn system. We expect that the second "intrinsic" spin J_ϕ^{Komar} will only be non-vanishing for the S^3 black hole, but that the black ring will also have non-vanishing angular velocity on the S^2. This would be interpreted as rotational dragging of the S^3 black hole on the black ring.

  The 3-soliton construction of section 2.2 does not give the most general doubly spinning black saturn configuration, because the black ring would not carry independent angular momentum on the S^2. The more general black saturn configuration should be possible to obtain with the methods recently used to construct the doubly spinning black ring [27].

  Doubly spinning black rings likely suffer from superradiant instabilities [43]. It would be interesting to see if such an instability is present also when the black ring is only being dragged on the S^2 by the S^3 black hole.

- *Dipole black saturn*: Black rings can carry non-conserved "dipole charges" [44]. Adding dipole charge(s) to the black ring will give a dipole black saturn solution. The techniques [45] for adding dipole charge by combining two or more vacuum solutions should apply here.

- *Charged black saturn*: Vacuum solutions can be charged up to carry conserved charges — and for black rings also dipole charges. Lifting the solutions to ten dimensions and using boosts and dualities it is easy to charge up Myers-Perry black holes and black rings to carry, say D1- and D5-charges. The same transformations give a D1-D5-charged black saturn configuration (although not the most general such solution). For black rings there is a technical difficulty in adding the third charge, momentum P, as detailed in [46]. This can be overcome by starting with a dipole black ring,

and in this way a class of non-supersymmetric three-charge black rings have been obtained [47].

Likewise, a D1-D5-P black saturn solution can be obtained from dipole black saturn, and this would lead to (a subclass of) non-supersymmetric generalizations of the supersymmetric concentric black ring solutions [15]. It would be interesting if techniques can be developed to add independent charges to multi-component black hole systems.

As discussed in the Introduction, one motivation for the existence of black saturn is to think of a thin black ring balanced in the external potential of the S^3 black hole. We have of course seen clear evidence of the gravitational interactions between the black ring and the S^3 black hole, for instance the rotational dragging (see section 4.3). So considering the black hole as providing an external potential should only be seen as a motivation for the case where the black ring is very thin with large S^1 radius so that the interactions between the objects is negligible. Following the method of [9] one can take the system off-shell and study the equilibrium of forces on a very thin black ring around a small black hole. Presumably this would give a Newtonian balance between a string-like tension of the ring and the angular velocity in the background gravitational potential of the S^3 black hole.

The balanced black saturn solution presented here has two separate sectors. These arise from two different ways of imposing the balance condition, as described in section 3. We have focused almost entirely on the sector where the Komar masses of both the black ring and the S^3 black hole are non-negative. However, the other sector — for which the S^3 black hole Komar mass is negative — may also contain interesting physics. We interpret the possibility of negative Komar mass as a consequence of extreme rotational dragging experienced by the S^3 black hole when its Komar angular momentum cannot counter the dragging by the black ring. It would be interesting to understand this strongly interacting system better.

The 3+1 dimensions double-Kerr solution can be constructed with methods similar to the ones used in this paper. While it is not possible for two Kerr-black holes to be balanced by spin-spin interactions alone, one could ask if it is for two Myers-Perry black holes in 4+1 dimensions. The static solution describing two (or more) Myers-Perry black holes held apart by conical singular membranes is easy to construct using the methods of [29]; this family of solutions was studied in [48]. Angular momentum can be added by soliton transformations similar to the ones used here. It is not clear if the resulting solution can be made free of singularities and, even if so, if the black holes can be held apart by the spin-spin interactions.

Little is known about what types of black holes are admitted by the Einstein equations in six and higher-dimensions. The main focus has been on spacetimes with a single connected black hole horizon, but black saturn has shown that interesting physics arises in higher-dimensional multi-black hole systems. It will be interesting to see what exotic multi-black hole solutions higher-dimensional gravity has to offer.

JHEP05(2007)050

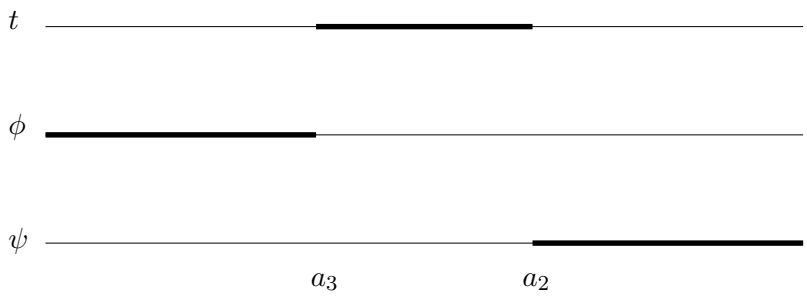

Figure 13: Sources for the Myers-Perry black hole. The timelike rod is aligned along $(1, 0, \Omega_\psi^{\rm BH})$.

Acknowledgments

We are grateful to Gary Horowitz, Harvey Reall, Enric Verdaguer and especially Roberto Emparan for discussions of the inverse scattering method and saturn physics. We thank Chethan Krishnan for pointing out that a clarification was needed for comparison of the results of the 2- and 3-soliton transformations.

PF would like to thank the Theoretical Physics group at Imperial College London for hospitality and also the Center for Theoretical Physics at MIT for warm hospitality while part of this work was done. HE thanks the Aspen Center for Physics for a fruitful stay during the summer 2006. HE also thanks the Theoretical Physics group at Uppsala University and the Niels Bohr Institute for hospitality during the final stages of this work.

HE was supported by a Pappalardo Fellowship in Physics at MIT and by the US Department of Energy through cooperative research agreement DE-FG0205ER41360. PF was supported by FI and BE fellowships from AGAUR (Generalitat de Catalunya), DURSI 2005 SGR 00082, CICYT FPA 2004-04582-C02-02 and EC FP6 program MRTN-CT-2004-005104.

A. Limits

In this section we provide details of the Myers-Perry black hole limit and the black ring limit of the black saturn solution.

A.1 Myers-Perry black hole

From the rod structure figure 2(b) of the full solution, one can see that the Myers-Perry black hole with a single angular momentum is obtained by eliminating the rod corresponding to the black ring. There is however an issue of the order of limits. First one can note that from our general saturn solution, with c_1 and c_2 arbitrary, the following two limits result in the same solution:

$$\text{Limit 1}: \quad a_1 \to a_5\,, \quad \text{then} \quad a_5 \to a_4\,,. \tag{A.1}$$

$$\text{Limit 2}: \quad a_5 \to a_4\,, \quad \text{then} \quad a_1 \to a_4\,,. \tag{A.2}$$

As long as c_1 and c_2 are kept fixed (i.e. the regularity condition (3.7) is *not* imposed), these two limits are equivalent and give the metric

$$\begin{aligned}
G_{tt} &= -\frac{\mu_3\left[-c_2^2\mu_2^2\mu_3+(\rho^2+\mu_2\mu_3)^2\right]}{\mu_2\left[c_2^2\mu_3\rho^2+(\rho^2+\mu_2\mu_3)^2\right]}\,, & G_{t\psi} &= -\frac{c_2\mu_3(\rho^2+\mu_2^2)(\rho^2+\mu_3^2)}{\mu_2\left[c_2^2\mu_3\rho^2+(\rho^2+\mu_2\mu_3)^2\right]}\,,\\
G_{\psi\psi} &= \frac{\mu_2^2(\rho^2+\mu_2\mu_3)^2-c_2^2\mu_3\rho^2}{\mu_2\left[c_2^2\mu_3\rho^2+(\rho^2+\mu_2\mu_3)^2\right]}\,, & G_{\phi\phi} &= \frac{\rho^2}{\mu_3}\,,\\
e^{2\nu} &= \frac{k^2\,\mu_2\left[c_2^2\mu_3\rho^2+(\rho^2+\mu_2\mu_3)^2\right]}{(\rho^2+\mu_2^2)(\rho^2+\mu_3^2)(\rho^2+\mu_2\mu_3)}\,.
\end{aligned} \tag{A.3}$$

To bring the metric given above to an asympotically flat form one has to perform change the coordinates according to $t = t' - c_2\psi'$ and $\psi = \psi'$. Finally, to show that this solution given in (A.3) is indeed the Myers-Perry black hole with a single angular momentum, one can change to prolate spheroidal coordinates as done in [30] and [21].

Now if we are interested in obtaining the Myers-Perry black hole as a limit of the black saturn configuration, we must remove the black ring in a limit where the condition (3.7) is imposed on c_1. Note that in Limit 1 of (A.1), $c_1 \to \infty$. This is the reason we consider Limit 2 in (A.1).

In the parametrization introduced in section 3.1 Limit 2 is

$$\kappa_3 \to \kappa_2\,, \quad \text{then} \quad \kappa_2 \to 0\,. \tag{A.4}$$

By first taking $\kappa_3 \to \kappa_2$ we eliminate the divergence in c_1 and then the $\kappa_2 \to 0$ limit can taken safely. The resulting metric is (A.3).

With $\bar{c}_2$ fixed by the balanced condition (3.17), this limit can only be taken for $\epsilon = +1$, and one finds

$$\bar{c}_2 = 1 - \frac{1}{2\kappa_1} \tag{A.5}$$

and all physical parameters are then functions of the dimensionless parameter κ_1 and the scale L, which are related to the standard Myers-Perry black hole parameters r_0 and a through

$$r_0^2 = \frac{L^2}{2\kappa_1}\,, \qquad a = \frac{L(1-2\kappa_1)}{\sqrt{2\kappa_1}}\,. \tag{A.6}$$

A.2 Black ring limit

The ψ-spinning black ring is obtained by first setting $c_2 = 0$, then taking $a_2 = a_3$. We must continue to impose the condition (3.7) for c_1; note that this condition is independent

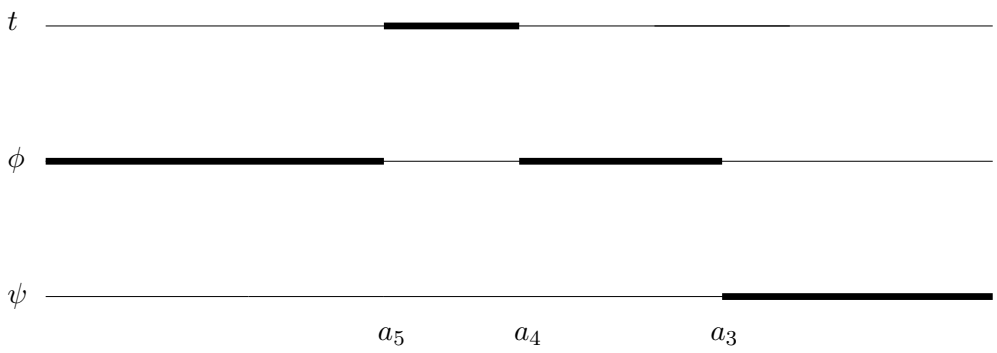

Figure 14: Sources for the black ring. The timelike rod has direction $(1, 0, \Omega_\psi^{\rm BR})$.

of a_2. We find

$$G_{tt} = -\frac{\mu_1\Big[\mu_5(\rho^2+\mu_1\mu_3)^2(\rho^2+\mu_1\mu_4)^2 - c_1^2\mu_3\mu_4(\mu_1-\mu_5)^2\rho^4\Big]}{\mu_4\Big[\mu_5(\rho^2+\mu_1\mu_3)^2(\rho^2+\mu_1\mu_4)^2 + c_1^2\mu_1^2\mu_3\mu_4(\mu_1-\mu_5)^2\rho^2\Big]}\,, \tag{A.7}$$

$$G_{t\psi} = -\frac{c_1\mu_3\mu_5(\mu_1-\mu_5)(\rho^2+\mu_1^2)(\rho^2+\mu_1\mu_3)(\rho^2+\mu_1\mu_4)}{\Big[\mu_5(\rho^2+\mu_1\mu_3)^2(\rho^2+\mu_1\mu_4)^2 + c_1^2\mu_1^2\mu_3\mu_4(\mu_1-\mu_5)^2\rho^2\Big]}\,, \tag{A.8}$$

$$G_{\psi\psi} = \frac{\mu_3\mu_5\Big[\mu_5(\rho^2+\mu_1\mu_3)^2(\rho^2+\mu_1\mu_4)^2 - c_1^2\mu_1^4\mu_3\mu_4(\mu_1-\mu_5)^2\Big]}{\mu_1\Big[\mu_5(\rho^2+\mu_1\mu_3)^2(\rho^2+\mu_1\mu_4)^2 + c_1^2\mu_1^2\mu_3\mu_4(\mu_1-\mu_5)^2\rho^2\Big]}\,, \tag{A.9}$$

$$e^{2\nu} = k^2\frac{\mu_3(\rho^2+\mu_1\mu_5)(\rho^2+\mu_3\mu_4)(\rho^2+\mu_4\mu_5)\Big[\mu_5(\rho^2+\mu_1\mu_3)^2(\rho^2+\mu_1\mu_4)^2+c_1^2\mu_1^2\mu_3\mu_4(\mu_1-\mu_5)^2\rho^2\Big]}{4\mu_1(\rho^2+\mu_1\mu_3)(\rho^2+\mu_1\mu_4)(\rho^2+\mu_3\mu_5)^2(\rho^2+\mu_1^2)(\rho^2+\mu_3^2)(\rho^2+\mu_4^2)(\rho^2+\mu_5^2)} \tag{A.10}$$

Note that for $c_1 = 0$ we obtain the metric for the static black ring. The corresponding rod structure is depicted in figure 14.

To verify that this solution really describes the ψ-ring, we rewrite the metric in ring coordinates (x, y), i.e.

$$\begin{aligned} ds^2 \;=\; & -\frac{F(y)}{F(x)}\left(dt + C_\lambda\, R\,\frac{1+y}{F(y)}d\psi\right)^2 \\ & + \frac{R^2}{(x-y)^2}F(x)\left[-\frac{G(y)}{F(y)}d\psi^2 - \frac{dy^2}{G(y)} + \frac{dx^2}{G(x)} + \frac{G(x)}{F(x)}d\phi^2\right], \end{aligned} \tag{A.11}$$

where

$$G(\xi) = (1-\xi^2)(1+\nu\xi)\,, \qquad F(\xi) = (1+\lambda\xi)\,, \qquad C_\lambda = \sqrt{\lambda(\lambda-\nu)\frac{1+\lambda}{1-\lambda}}\,. \tag{A.12}$$

The coordinate transformation from Weyl coordinates (ρ, z) to ring coordinates (x, y) is

$$\rho = \frac{R^2\sqrt{-G(x)G(y)}}{(x-y)^2}\,, \qquad z = \frac{R^2(1-xy)[2+\nu(x+y)]}{2(x-y)^2}\,. \tag{A.13}$$

Note that

$$d\rho^2 + dz^2 = K(x,y)\left[-\frac{dy^2}{G(y)} + \frac{dx^2}{G(x)}\right], \tag{A.14}$$

with

$$K(x,y) = -\frac{R^4}{4(x-y)^3}[x+y+\nu(1+xy)][2+\nu(1+x+y-xy)][2+\nu(-1+x+y+xy)]\,. \tag{A.15}$$

The rod endpoints are related to the parameters ν and λ as

$$a_1 = R^2\alpha\,, \quad a_5 = -\frac{R^2}{2}\nu\,, \quad a_4 = \frac{R^2}{2}\nu\,, \quad a_3 = \frac{R^2}{2}\,. \tag{A.16}$$

Here $\alpha < -\nu/2$ is a constant which will be determined below. With this choice, $\rho^2+(z-a_i)^2$ is a perfect square for $i = 3,4,5$ (but not for $i = 1$ for choice of $\alpha < -\nu/2$) so we have simple expressions for $\mu_i = R_i - (z-a_i) = \sqrt{\rho^2+(z-a_i)^2} - (z-a_i)$:

$$\mu_5 = -\frac{R^2(1-x)(1+y)(1+\nu y)}{(x-y)^2}\,, \tag{A.17}$$

$$\mu_4 = -\frac{R^2(1-x)(1+y)(1+\nu x)}{(x-y)^2}\,, \tag{A.18}$$

$$\mu_3 = -\frac{R^2(1-y^2)(1+\nu x)}{(x-y)^2}\,. \tag{A.19}$$

The expression for μ_1, however, involves an explicit squareroot, $R_1 = \sqrt{\rho^2+(z-a_1)^2}$. We write $\mu_1 = R_1 - (z-a_1)$, but keep R_1 unevaluated. Then collect powers of R_1 and simplify the expressions for each metric component when only even powers of R_1 are replaced by their expression in terms of x, y. Then we end up in general for each metric component with expressions of the form

$$g_{\mu\nu} \sim \frac{p_0 + p_1 R_1}{q_0 + q_1 R_1}\,, \tag{A.20}$$

where $p_{0,1}$ and $q_{0,1}$ are functions of x, y. Now it turns out, as can explicitly be verified, that for all cases, $p_0/q_0 = p_1/q_1$ so that $g_{\mu\nu} = p_0/q_0$. Thus we have eliminated the squareroot R_1 from the expressions, and indeed p_0/q_0 is a simple function of x, y. For example, we find

$$G_{tt} = -\frac{2-2\alpha(1+y)-\nu(1-y)}{2-2\alpha(1+x)-\nu(1-x)}\,. \tag{A.21}$$

We bring G_{tt} to the standard from given in (A.11) by choosing

$$\alpha = \frac{\nu(1+\lambda)-2\lambda}{2(1-\lambda)}\,. \tag{A.22}$$

The condition that $\alpha \leq -\nu/2$ is then simply that $\nu \leq \lambda$, while $-\infty < \alpha$ gives $\lambda < 1$. We have therefore recovered the bound

$$0 < \nu \leq \lambda < 1 \tag{A.23}$$

on the black ring parameters λ and ν.

With this choice (A.22) for α we have

$$e^{2\nu} = \frac{k^2(1-\nu)^2}{1-\lambda}\frac{R^2}{(x-y)^2}\frac{F(x)}{K(x,y)}\,, \tag{A.24}$$

so that choosing the integration constant k as

$$k^2 = \frac{(1-\lambda)}{(1-\nu)^2} \tag{A.25}$$

we recover the x, y-part of the metric (A.11). With these choices for α (the position of the "fake" rod endpoint) and k, the full metric (A.7) becomes (A.11).

Note that in the black ring limit with $\bar{c}_2 = 0$, the periods (3.15) are $\Delta\psi = \Delta\phi = 2\pi k$, which with k given above agrees precisely with the result for the black ring [44]. Likewise all physical parameters of the neutral black ring are reproduced from this limit of the black saturn solution.

References

[1] S.D. Majumdar, *A class of exact solutions of Einstein's field equations*, *Phys. Rev.* **72** (1947) 390;
A. Papapetrou, *A static solution of the equations of the gravitational field for an arbitrary charge distribution*, *Proc. Roy. Irish Acad.* **A51** (1947) 191;
J.B. Hartle and S.W. Hawking, *Solutions of the Einstein-Maxwell equations with many black holes*, *Commun. Math. Phys.* **26** (1972) 87.

[2] D. Kramer and G. Neugebauer, *The superposition of two Kerr solutions*, *Phys. Lett.* **A 75** (1980) 259.

[3] R. Wald, *Gravitational spin interaction*, *Phys. Rev.* **D 6** (1972) 406.

[4] C. Hoenselaers, *Remarks on the Double-Kerr solution*, *Prog. Theor. Phys.* **72** (1984) 761.

[5] W. Dietz and C. Hoenselaers, *Two mass solutions of Einstein's vacuum equations: the double Kerr solution*, *Ann. Phys. (N.Y.)* **165** (1985) 319.

[6] V.S. Manko and E. Ruiz, *Exact solution of the double-Kerr equilibrium problem*, *Class. Quant. Grav.* **18** (2001) L11.

[7] H. Stephani, D. Kramer, M. MacCallum, C. Hoenselaers and E. Herlt, *Exact solutions of Einstein's field equations*, Cambridge University Press, Cambridge (2003).

[8] R. Emparan and H.S. Reall, *A rotating black ring in five dimensions*, *Phys. Rev. Lett.* **88** (2002) 101101 [hep-th/0110260]; See also the review: *Black rings*, *Class. and Quant. Grav.* **23** (2006) R169 [hep-th/0608012].

[9] H. Elvang, R. Emparan and A. Virmani, *Dynamics and stability of black rings*, *JHEP* **12** (2006) 074 [hep-th/0608076].

[10] J.L. Hovdebo and R.C. Myers, *Black rings, boosted strings and Gregory-Laflamme*, *Phys. Rev.* **D 73** (2006) 084013 [hep-th/0601079].

[11] R.C. Myers and M.J. Perry, *Black holes in higher dimensional space-times*, *Ann. Phys. (NY)* **172** (1986) 304.

[12] G.W. Gibbons, D. Ida and T. Shiromizu, *Uniqueness and non-uniqueness of static vacuum black holes in higher dimensions*, *Prog. Theor. Phys. Suppl.* **148** (2003) 284 [gr-qc/0203004]; S. Hwang, *A rigidity theorem for Ricci flat metrics*, *Geometriae Dedicata* **71** (1998) 5.

[13] H. Kodama, *Perturbative uniqueness of black holes near the static limit in arbitrary dimensions*, *Prog. Theor. Phys.* **112** (2004) 249 [hep-th/0403239].

[14] H. Elvang, R. Emparan and P. Figueras, *Phases of five-dimensional black holes*, hep-th/0702111.

[15] J.P. Gauntlett and J.B. Gutowski, *Concentric black rings*, *Phys. Rev.* **D 71** (2005) 025013 [hep-th/0408010]; *General concentric black rings*, *Phys. Rev.* **D 71** (2005) 045002 [hep-th/0408122].

[16] J.P. Gauntlett, J.B. Gutowski, C.M. Hull, S. Pakis and H.S. Reall, *All supersymmetric solutions of minimal supergravity in five dimensions*, *Class. and Quant. Grav.* **20** (2003) 4587 [hep-th/0209114].

[17] J.B. Gutowski, D. Martelli and H.S. Reall, *All supersymmetric solutions of minimal supergravity in six dimensions*, *Class. and Quant. Grav.* **20** (2003) 5049 [hep-th/0306235].

[18] V.A. Belinsky and V.E. Zakharov, *Integration of the Einstein equations by the inverse scattering problem technique and the calculation of the exact soliton solutions*, *Sov. Phys. JETP* **48** (1978) 985 [*Zh. Eksp. Teor. Fiz.* **75** (1978) 1953].

[19] V.A. Belinsky and V.E. Sakharov, *Stationary gravitational solitons with axial symmetry*, *Sov. Phys. JETP* **50** (1979) 1 [*Zh. Eksp. Teor. Fiz.* **77** (1979) 3].

[20] V. Belinski and E. Verdaguer, *Gravitational solitons*, Cambridge University Press, Cambridge, (2001).

[21] A.A. Pomeransky, *Complete integrability of higher-dimensional Einstein equations with additional symmetry and rotating black holes*, *Phys. Rev.* **D 73** (2006) 044004 [hep-th/0507250].

[22] T. Mishima and H. Iguchi, *New axisymmetric stationary solutions of five-dimensional vacuum Einstein equations with asymptotic flatness*, *Phys. Rev.* **D 73** (2006) 044030 [hep-th/0504018].

[23] S. Tomizawa, Y. Morisawa and Y. Yasui, *Vacuum solutions of five dimensional Einstein equations generated by inverse scattering method*, *Phys. Rev.* **D 73** (2006) 064009 [hep-th/0512252].

[24] P. Figueras, *A black ring with a rotating 2-sphere*, *JHEP* **07** (2005) 039 [hep-th/0505244].

[25] H. Iguchi and T. Mishima, *Solitonic generation of five-dimensional black ring solution*, *Phys. Rev.* **D 73** (2006) 121501 [hep-th/0604050].

[26] S. Tomizawa and M. Nozawa, *Vaccum solutions of five-dimensional Einstein equations generated by inverse scattering method. II: production of black ring solution*, *Phys. Rev.* **D 73** (2006) 124034 [hep-th/0604067].

[27] A.A. Pomeransky and R.A. Sen'kov, *Black ring with two angular momenta*, hep-th/0612005.

[28] H. Kudoh, *Doubly spinning black rings*, *Phys. Rev.* **D 75** (2007) 064006 [gr-qc/0611136].

[29] R. Emparan and H.S. Reall, *Generalized Weyl solutions*, *Phys. Rev.* **D 65** (2002) 084025 [hep-th/0110258].

JHEP05(2007)050

[30] T. Harmark, *Stationary and axisymmetric solutions of higher-dimensional general relativity*, *Phys. Rev.* **D 70** (2004) 124002 [hep-th/0408141].

[31] H. Elvang, R. Emparan, D. Mateos and H.S. Reall, *A supersymmetric black ring*, *Phys. Rev. Lett.* **93** (2004) 211302 [hep-th/0407065].

[32] I. Bena and N.P. Warner, *One ring to rule them all ... and in the darkness bind them?*, *Adv. Theor. Math. Phys.* **9** (2005) 667 [hep-th/0408106].

[33] H. Elvang, R. Emparan, D. Mateos and H.S. Reall, *Supersymmetric black rings and three-charge supertubes*, *Phys. Rev.* **D 71** (2005) 024033 [hep-th/0408120].

[34] J. Kunz and F. Navarro-Lerida, *Non-uniqueness, counterrotation and negative horizon mass of Einstein-Maxwell-Chern-Simons black holes*, *Mod. Phys. Lett.* **A 21** (2006) 2621 [hep-th/0610075].

[35] M. Cvetič, G.W. Gibbons, H. Lu and C.N. Pope, *Rotating black holes in gauged supergravities: thermodynamics, supersymmetric limits, topological solitons and time machines*, hep-th/0504080.

[36] J.C. Breckenridge, R.C. Myers, A.W. Peet and C. Vafa, *D-branes and spinning black holes*, *Phys. Lett.* **B 391** (1997) 93 [hep-th/9602065].

[37] H. Elvang and G.T. Horowitz, *When black holes meet Kaluza-Klein bubbles*, *Phys. Rev.* **D 67** (2003) 044015 [hep-th/0210303].

[38] J.P. Gauntlett, R.C. Myers and P.K. Townsend, *Black holes of $D = 5$ supergravity*, *Class. and Quant. Grav.* **16** (1999) 1 [hep-th/9810204].

[39] K. Copsey and G.T. Horowitz, *The role of dipole charges in black hole thermodynamics*, *Phys. Rev.* **D 73** (2006) 024015 [hep-th/0505278].

[40] D. Astefanesei and E. Radu, *Quasilocal formalism and black ring thermodynamics*, *Phys. Rev.* **D 73** (2006) 044014 [hep-th/0509144].

[41] G. Arcioni and E. Lozano-Tellechea, *Stability and critical phenomena of black holes and black rings*, *Phys. Rev.* **D 72** (2005) 104021 [hep-th/0412118]; *Stability and thermodynamics of black rings*, hep-th/0502121.

[42] R. Gregory and R. Laflamme, *Black strings and p-branes are unstable*, *Phys. Rev. Lett.* **70** (1993) 2837 [hep-th/9301052]; *The instability of charged black strings and p-branes*, *Nucl. Phys.* **B 428** (1994) 399 [hep-th/9404071];
T. Harmark, V. Niarchos and N.A. Obers, *Instabilities of black strings and branes*, *Class. and Quant. Grav.* **24** (2007) R1 [hep-th/0701022].

[43] O.J.C. Dias, *Superradiant instability of large radius doubly spinning black rings*, *Phys. Rev.* **D 73** (2006) 124035 [hep-th/0602064].

[44] R. Emparan, *Rotating circular strings and infinite non-uniqueness of black rings*, *JHEP* **03** (2004) 064 [hep-th/0402149].

[45] S.S. Yazadjiev, *Completely integrable sector in 5D Einstein-Maxwell gravity and derivation of the dipole black ring solutions*, *Phys. Rev.* **D 73** (2006) 104007 [hep-th/0602116]; *Solution generating in 5d Einstein-Maxwell-dilaton gravity and derivation of dipole black ring solutions*, *JHEP* **07** (2006) 036 [hep-th/0604140]; *Rotating dyonic dipole black rings: exact solutions and thermodynamics*, *Gen. Rel. Grav.* **39** (2007) 601 [hep-th/0607101].

JHEP05(2007)050

[46] H. Elvang and R. Emparan, *Black rings, supertubes and a stringy resolution of black hole non-uniqueness*, *JHEP* **11** (2003) 035 [hep-th/0310008].

[47] H. Elvang, R. Emparan and P. Figueras, *Non-supersymmetric black rings as thermally excited supertubes*, *JHEP* **02** (2005) 031 [hep-th/0412130].

[48] H.S. Tan and E. Teo, *Multi-black hole solutions in five dimensions*, *Phys. Rev.* **D 68** (2003) 044021 [hep-th/0306044].